Extensive longevity and DNA virus-driven adaptation in nearctic *Myotis* bats

Juan M Vazquez[1,2,20], M. Elise Lauterbur[3,4,20], Saba Mottaghinia[5], Léa Gaucherand[6], Sarah Maesen[5], Michael Singer[7], Sarah Villa[7], Melanie Bucci[3], Devaughn Fraser[8,9], Genavieve Gray-Sandoval[3], Zeinab R Haidar[10,111], Melissa Han[12], William Kohler[12], Tanya M. Lama[13], Amandine Le Corf[5], Clara Loyer[5], Dakota McMillan[1,14], Stacy Li[1,15], Johnathan Lo[15], Carine Rey[5], Samantha LR Capel[8], Kathleen Slocum[16], Melissa Sui[7], William Thomas[17], Janet Debelak Tyburec[18], Rachel Brem[19], Richard Miller[12], Michael Buchalski[8], Jose Pablo Vazquez-Medina[1], Sébastien Pfeffer[6], Lucie Etienne[6,21]*, David Enard[3,21,22]**, Peter H Sudmant[1,14,21,22,23]***

Affiliations:

1. Department of Integrative Biology, University of California, Berkeley, Berkeley, CA USA
2. Current affiliation: Department of Biology, Pennsylvania State University, State College, PA USA
3. Department of Ecology and Evolutionary Biology, University of Arizona, Tucson, AZ USA
4. Current affiliation: Department of Biology, University of Vermont, Burlington, VT USA
5. Centre International de Recherche en Infectiologie (CIRI), Inserm U1111, UCBL1, CNRS UMR5308, Ecole Normale Supérieure ENS de Lyon, Université de Lyon, Lyon, France
6. Université de Strasbourg, Architecture et Réactivité de l'ARN, Institut de Biologie Moléculaire et Cellulaire du CNRS, Strasbourg, France.
7. Department of Molecular and Cellular Biology, University of California, Berkeley, Berkeley, CA USA
8. Wildlife Genetics Research Unit, Wildlife Health Laboratory, California Department of Fish and Wildlife, Sacramento, CA, USA
9. Current affiliation: Wildlife Diversity Program, Wildlife Division, Connecticut Department of Energy and Environmental Protection, Burlington, CT, USA
10. Department of Biology, California State Polytechnic University, Humboldt, Arcata, CA USA
11. Current affiliation: Western EcoSystems Technology Inc, Cheyenne, WY USA
12. Department of Pathology and Clinical Laboratories, University of Michigan, Ann Arbor, MI USA
13. Department of Biological Sciences, Smith College, Northampton, MA USA
14. Department of Science and Biotechnology, Berkeley City College, Berkeley, CA USA
15. Center for Computational Biology, University of California, Berkeley, Berkeley, CA USA
16. Bat Conservation International, Austin, TX USA
17. Department of Ecology and Evolution, Stony Brook University, Stony Brook NY USA
18. Bat Survey Solutions, LLC, Tucson, AZ USA
19. Department of Plant and Microbial Biology, University of California, Berkeley, Berkeley, CA 94720, USA
20. These authors contributed equally
21. Senior author
22. These authors contributed equally
23. Lead contact

* Correspondence: lucie.etienne@ens-lyon.fr
** Correspondence: denard@arizona.edu

*** Correspondence: psudmant@berkeley.edu

Summary Paragraph

The genus *Myotis* is one of the largest clades of bats, and exhibits some of the most extreme variation in lifespans among mammals alongside unique adaptations to viral tolerance and immune defense[1–5]. To study the evolution of longevity-associated traits and response to infectious disease, we generated cell lines and near-complete genome assemblies for 8 closely related species of *Myotis*. Using genome-wide screens of positive selection, analyses of structural variation, and functional experiments in primary cells, we identify new patterns of adaptation contributing to longevity, cancer resistance, and viral interactions in bats. We demonstrate distinct modes of adaptation to DNA and RNA viruses in bats, with bats demonstrating genome-wide overrepresentation of positive selection for DNA virus-interacting proteins, and significant rates of copy number variation for RNA virus-interacting proteins, in contrast to other mammals. We show that the recurrent evolution of longevity seen in *Myotis* leads to pervasive positive selection in cancer pathways, and demonstrate a unique response to DNA damage in primary cells of the long-lived *M. lucifugus*. Together, our results suggest that bats' remarkable longevity and immunity are linked through pleiotropic adaptations against viruses and aging-related disease.

Keywords

Aging, Bats, Cancer, Evolutionary Biology, Functional Genomics, Immunity, Infectious Disease

Introduction

Bats (order *Chiroptera*) represent approximately 20% of all known mammalian species and are one of the most phenotypically diverse clades of mammals[6,7]. Since their emergence 60 million years ago[8–10], many bat lineages have independently evolved a wide variety of life history strategies and phenotypic traits, including exceptional changes in longevity, viral tolerance, and immune defense[1,4,11–14]. Such systems, in which shared traits have evolved *de novo* multiple times, are powerful resources for dissecting the genetic basis of phenotypes. Rigorous approaches to studying these traits, however, depend on high-quality, well-annotated genomes to test evolutionary and genomic hypotheses, and on experimental functional systems to validate these hypotheses.

The largest genus of bats - *Myotis* - is estimated to have emerged approximately 33 million years ago[15,16], and encompasses over 139 described species spanning six continents and a wide range of ecological niches[6,15–17]. *Myotis* species demonstrate some of the most extreme variation in lifespan amongst mammals[1,2,18–20], including a six-fold difference in lifespan between the longest-lived species (*M. brandtii*, 42 years[18,21], **Fig. 1A**) and the shortest-lived species (*M. nigricans*, 7 yrs[18,22]) which diverged approximately 10.6 million years ago[10,17,23,24]. In addition, *Myotis* species have been used as systems for investigating virus tolerance and other pathogen resistance[25–27] associated with the expansion and contraction of antiviral defenses[28–31], which have contributed to bats' ecological role as zoonotic reservoirs[3,4,13,32–34].

While studies on the genetic basis of longevity in short-lived model organisms have been crucial for identifying and dissecting several key aging pathways, comparative studies of exceptionally long-lived

organisms have uncovered novel genes and pleiotropic effects governing lifespan[35–48]. Similarly, studies of infectious disease response are common and powerful in model organisms, but the lack of diversity and use of inbred lines limits their scope. Bats in particular present an important case study in, and opportunity to study, variation in virus adaptation strategies due to bats' role as zoonotic reservoirs and their specific resistance to viruses[44,49].

Here we combined comparative and functional approaches in *Myotis* to uncover genomic and functional evidence of adaptation to both aging-related and infectious diseases. Using near-complete genome assemblies, we identified significant structural variation encompassing stress response, immunity, and inflammation genes, including a trans-species copy number polymorphism of Protein kinase R (PKR). Additionally, we quantify the rates of evolution in body size and lifespan across mammals and find that both ancestral and extant *Myotis* species are overrepresented at the extreme of increased lifespan. Consistent with this observation, we identified pervasive selection of genes in longevity- and cancer-related processes throughout *Myotis*. We observed some of the strongest signatures of selection at immune-related genes, including strong evidence of adaptation in virus-interacting proteins in *Myotis* and other bats. In contrast to humans and other primates, in which virus adaptation is driven by interactions with RNA viruses[50], we find that virus adaptation in bats is driven by interactions with DNA viruses, implying that bats' exceptional immune adaptations are more protective against DNA viruses. This also highlights a fundamental discordance between the fitness impacts of viruses on humans vs bats. Together, our results suggest that pleiotropy and co-evolution of traits in *Myotis* has played a key role in the evolution of exceptional longevity and infectious disease resistance.

Results

High quality chromosome-level assemblies of 8 *Myotis* bat species

To study how lifespan and viral response have evolved in *Myotis*, we collected skin punches and derived primary cell lines from several North American ("nearctic")[23] species (**Fig. 1A,C),** including from one of the longest-lived mammals, *Myotis lucifugus*[18]. Using these cell lines and flash frozen tissues we generated *de novo* haplotype-resolved, chromosome-scale genome assemblies for eight species (**Fig. 1A, Extended Data Fig. 1**) using a combination of long-read PacBio HiFi sequencing and HiC scaffolding. These genomes are highly contiguous, with an average of 98.6% of nucleotides assembled into 22-23 syntenic chromosome-scale scaffolds corresponding to the published karyotype[51] with an average QV of 66 (Extended Data Fig. 1; **Extended Data Table 1**). These genomes have among the highest contig NG50 and lowest auNG scores of any *Chiroptera* genome published to date (**Fig. 1A, E**; **Extended Data Fig. 1**; **Extended Data Table 1**). We identified an average of 20,869 protein coding genes with mammalian homologs per genome, with BUSCO[52,53] scores ranging from 98.2% to 98.5% (**Fig. 1D**). Using these annotations, we examined the conflicting phylogenies within nearctic *Myotis*[15,17,54–57] by using 1-to-1 orthologs of protein-coding genes across 536 mammalian genomes (**Extended Data Table 2**) to build a time-calibrated, maximum likelihood tree of *Eutheria*. Our results conclusively resolve the relationship between sister taxa (*M. lucifugus* and *M. occultus*; *M. yumanensis and M. velifer*; and *M. evotis* and *M. thysanodes*) with both 100% bootstrap support and 100% Local Posterior Probability (LPP) scores at all nodes within nearctic *Myotis*. However, the root of nearctic *Myotis* remains unresolved with 0% LPP support despite 100% bootstrapping support, although our placement of the nearctic common ancestor as sister to *Myotis brandtii* is supported by geography and recent work in the literature[56–58]. (**Fig. 1B**; **Extended Data Fig. 2A**; **Extended Data Table 1**)

Across all 8 genomes, each autosome has been completely assembled telomere-to-telomere (T2T) in at least one species (**Fig. 1E**). Within assemblies, 29%-70% of chromosomes are fully assembled with an average of less than one gap per chromosome (**Extended Data Table 1**). Overall, these fully annotated genomes represent some of the most contiguous mammalian assemblies to date.

Evolution of structural variation within constrained karyotypes

With our near-complete assemblies, we first sought to study the landscape of structural variation within the tightly-conserved karyotype seen in *Myotis*. With only six exceptions across over 60 studied species[59–63], all *Myotis* species have a conserved 2n=42 karyotype - a remarkable phenomenon for a genus spread across six continents and 33 million years of divergence[6,7,16,51]. The conserved *Myotis* karyotype consists of three large autosomes and one small metacentric autosome; 17 small telocentric autosomes; and metacentric X and Y chromosomes[51,64]. Consistent with this broad cytological conservation, we find large scale synteny across the nearctic *Myotis* in this study (**Fig. 2A**). However, structural variants (SVs) including inversions, duplications, and translocations are relatively common within chromosomes, especially adjacent to putative centromeric regions (**Fig. 2A, B**). This includes a ~20Mb block at the sub-telomeric end of Chr V15 that displays frequent and recurrent inversions and translocations across the nearctic *Myotis*, and which contains a 10Mb locus that was recently identified as a potential target of recent selection by adaptive introgression[57] (**Extended Data Fig. 3D**).

Using SyRI[65], we identified between 6,813 - 8,013 SVs per nearctic *Myotis* genome relative to their outgroup, *M. myotis*; 97 - 99% of these events were under 10Kb. In the three large autosomes, which constitute ~30% of the genome, we cataloged an average of 509 SVs (**Extended Data Table 3**). In contrast, in the small autosomes, constituting ~65% of the genome, we observed an average of 316 events, highlighting the distinct structural evolution between these chromosome types with SVs found at 2-fold higher density in larger autosomes (**Extended Data Table 3**). However, large (≥10Kb) duplications, large inverted duplications, and large inverted translocations were more common on small autosomes compared to the large autosomes (**Extended Data Table 3**). We also quantified the distribution of transposable elements (TEs) across chromosomes (**Fig. 2B,C**). Consistent with prior observations in other Chiropteran genomes[66], LINE elements appeared to be enriched around the predicted centromere (**Fig. 2B**) with simulations showing that this trend is primarily limited to the long, metacentric autosomes (**Extended Data Fig. 3A**; **Extended Data Table 3**). The concentration of segmental duplications was also significantly correlated with TE density in each species (linear regression, $p < 0.001$; **Fig. 2B,D; Extended Data Fig. 3B**) highlighting the importance of TEs in facilitating structural evolution. Together these results highlight high levels of structural variation coincident with mobile element activity occurring in the context of a highly constrained karyotype.

An actively segregating, trans-species copy number polymorphism of the antiviral factor Protein Kinase R, PKR

Among the structural variants identified in nearctic *Myotis*, the gene Protein Kinase R (*PKR*/*EIF2AK2*) stood out as an interferon-stimulated gene with antiviral activity against both DNA and RNA viruses. While the functionality of this *Myotis*-specific duplication had been previously characterized[30], the absence of long-read sequencing data for *Myotis* has prevented a more detailed characterization of copy number and evolutionary history among Neartic *Myotis.* Using our near-complete genome assemblies, we fully resolved the sequence and structure of the two previously known haplotypes: H1, containing a single copy of *PKR*

157 (*PKR2*); and H2, containing two tandemly duplicated copies of *PKR* (*PKR1* and *PKR2*; **Fig. 3A**). We also
158 identified a third haplotype - H3 - with three tandem duplicates of *PKR* (*PKR1*, *PKR2*, and a third copy)
159 present only in *M. californicus*. Remarkably, while 7 out of 9 *Myotis* species carried duplicated haplotypes, 5
160 of these cases were heterozygous for the duplicated haplotype (i.e. H1/H2 or H1/H3; **Fig. 3B**). Two *Myotis*
161 individuals (*lucifugus* and *evotis*) only carried non-duplicated (i.e. H1/H1; **Fig. 3B**). To determine the
162 evolutionary history of the duplicates, we used GeneRax[67] to construct a tree from alignments of all *PKR*
163 gene copies across Neartic *Myotis*, using *Pipistrellus pygmaeus* as a non-*Myotis* outgroup (**Fig. 3C**). Our
164 results suggest that *PKR2* is the ancestral copy of *PKR*, and that *PKR1* originated from a single duplication
165 event at the root of *Myotis*. These results highlight that both the duplicated and unduplicated haplotypes have
166 likely been segregating for tens of millions of years, representing an ancient trans-species polymorphism.

167 PKR is a stress response and innate immune factor that becomes active upon detection of dsRNA
168 through sensing, auto-phosphorylation and dimerization[68,69]. Active PKR shuts down protein translation and
169 restricts viral replication[68,69]. Although PKR1 and PKR2 are both expressed in basal or interferon-stimulated
170 *Myotis velifer* cells, only their independent functional impacts have previously been investigated[30]. Given the
171 co-expression and the complex haplotype diversity we identified in *Myotis*, we set out to determine whether
172 the two *PKR* copies act additively, synergistically, or as dominant negatives in several essential functions.
173 We therefore investigated the functional impact of the duplicates' co-expression on total PKR protein
174 expression levels, cell viability, inhibition of translation, antiviral restriction and homo/hetero-dimer formation
175 (**Fig. 3D-H**). To pinpoint the contribution of PKRs, we used a heterologous cell system[30] with PKR-KO Hela
176 cells transfected with either an empty pSG5 plasmid (control), or pSG5 encoding PKR1, PKR2, or
177 PKR1+PKR2 (1:1 ratio) from *Myotis myotis* (myoMyo) or *Myotis velifer* (myoVel). In this system, PKR
178 transfection leads to its autoactivation[30]. First, we investigated PKR protein expression and found that,
179 although *Myotis* Flag-PKR1 was expressed at lower levels than Flag-PKR2, PKR1+PKR2 co-expression did
180 not affect the overall PKRs' steady-state protein expression levels (**Extended Data Fig. 4A**).

181 Second, we performed cell viability assays at two doses of transfected PKRs and found that cell
182 viability was only affected at high dose (**Extended Data Fig. 4D**). Third, using a luciferase reporter
183 translational assay, we found that PKR1+PKR2 coexpression led to an intermediate translation shutdown,
184 showing neither synergistic nor dominant negative effect of the PKR duplicates (**Fig. 3D**). Fourth, we tested
185 PKR1+PKR2 co-expression effects on infections by two different model RNA viruses: VSV-GFP (Vesicular
186 stomatitis virus encoding a GFP reporter[70], a representative of *Rhabdoviridae* family that is common in bats,
187 including *Myotis*) and SINV-GFP (Sindbis virus, a representative of *Togaviridae*) (**Fig. 3E-F**, **Extended Data**
188 **Fig. 4C,E**). We found that PKR1+PKR2 restricted viral infections to a similar, though slightly higher, extent
189 as PKR1 or PKR2 alone (**Fig. 3E-F; Extended Data Fig. 4C-D**, $p>0.05$). While the recently duplicated PKR1s
190 homodimerized, PKR1 and PKR2 did not form heterodimers (**Fig. 3G-H**, **Extended Data Fig. 4B** in SINV
191 condition). This suggests that, since their duplication, divergence between *Myotis* PKR copies has been
192 particularly strong at the protein-protein interface hindering their capacity to form heterodimers.

193 Together, these results suggest that PKR1 and PKR2 are neither dominant negative nor synergistic
194 with each other, but rather act in a mostly additive form for their main cellular effector functions. Despite their
195 capacity to more broadly escape some DNA and RNA viral antagonists[30], increased cell toxicity at high PKR
196 dose suggests a possible tradeoff upon PKR duplication, which might participate in also explaining why PKR
197 is rarely duplicated in mammals. Consistent with this, PKR1, which is generally more potent in our
198 experiments, is expressed at significantly lower levels in *Myotis velifer* cells than PKR2[30]. Altogether, these
199 genomic and functional results unveil gene duplicates still segregating across several *Myotis* species,
200 possibly shaped by recent viral infections and cell toxicity tradeoff.

Genome-wide adaptation to DNA viruses

To further explore how viruses may have shaped the genomes of *Myotis* bats we tested for adaptive signatures in virus-interacting proteins (VIPs) in *Myotis* and other bats. VIPs are host proteins that physically interact with viral proteins (e.g. *CD45*, **Fig. 4A**), and can be proviral (contributing to viral infection, e.g. viral receptors), antiviral (protective against viral infection, e.g. interferons), or both depending on infection stage and virus type. VIPs commonly have major roles in basic host function, and as a result most host cell biological pathways include VIPs. Previous studies investigating positive selection across mammals have found an enrichment for adaptation among a set of 5,527 manually curated VIPs, defined as host proteins that have at least one experimentally verified physical interaction with a viral protein, RNA, or DNA[71].

By calculating an enrichment score from the ratio of positive selection in VIPs compared to their matched control genes using BUSTED-MH[72], we found that, like other mammals, *Myotis* show an enrichment for adaptation at VIPs (**Fig. 4D; Extended Data Table 5**). Physical host-virus interactions may not always result in fitness effects in the host. We therefore repeated our analysis using a gene set restricted to VIPs with experimental evidence of specific pro- or anti-viral effects, and thus with a stronger expectation of fitness effects. We expect that if viruses were not the primary driver of adaptation in VIPs, then there would be no difference in the enrichment of selection in VIPs with vs without demonstrated pro- or anti-viral effects. We observed an even stronger significant elevation in the ratio of positive selection in these proviral and antiviral VIPs (**Fig. 4B; Extended Data Table 5**), but no elevation in this ratio in VIPs without experimental evidence of specific pro- or anti-viral effects (**Fig. 4C; Extended Data Table 5**). This is consistent with the expectation of viral interaction as the cause of enrichment of positive selection in VIPs in bats[73]. We repeated this analysis using a dataset of 47 publicly-available non-*Myotis* bat genomes, and confirmed these same patterns across bats more broadly, even when excluding *Myotis* genomes (**Extended Data Fig. 5A**).

Previous work has suggested that bats may have different physiological responses to DNA and RNA viruses[74]. To determine if this was reflected in genomic VIP adaptation, we compared the enrichment of positive selection in VIPs that interact only with DNA viruses (DNA-only VIPs) to those that interact only with RNA viruses (RNA-only VIPs). Remarkably, we found that VIP adaptation in *Myotis* and other bats is driven by selection in DNA VIPs (**Fig. 4E, Extended Data Fig. 5B**) in marked contrast to the observed pattern in RNA VIPs, which show no evidence of genome-wide enrichment in adaptation (**Fig. 4F, Extended Data Fig. 5C**).

Adaptation to viral pathogens can also occur via gene copy number changes[75,76,77,78]. We tested whether VIPs were enriched among genes that were recently gained or lost throughout *Myotis* using the method of Huang *et al*. (2023) to test the cumulative per gene, per branch copy number changes and birth-death rates of VIPs compared to other non-VIP genes.[42] While the birth-death rate of VIP genes overall was no different than non-VIP genes ($p = 0.071$, **Extended Data Fig. 5D**), VIP genes were significantly more likely to have undergone expansions and/or contractions on at least one branch of the *Myotis* family ($p < 0.001$; **Fig. 4G**). Furthermore, we find that this pattern is driven exclusively by copy number changes in RNA-only VIPs, and not by changes in copy number of DNA-only VIPs (**Fig. 4H-I)**. This suggests that there is variation in gene family birth rates across species, but that VIPs are more dynamic across the nearctic *Myotis* as a whole than other types of genes highlighting the importance of the viral immune response in recent *Myotis* evolution.

In contrast to what we observe in bats, VIP adaptation in humans is driven by positive selection in RNA - and not DNA - VIPs[71,79]. To investigate if DNA VIP-driven adaptation in bats is exceptional among

mammals, we replicated these analyses across four other large mammalian orders that are well represented among publicly-available mammalian genomes: *Primates*, *Glires*, *Euungulata*, and *Carnivora*. We found that while other mammalian orders show a mix of adaptation enrichments in both RNA and DNA VIPs, none show an absence of genome-wide enrichment of adaptation in RNA VIPs as observed in bats (**Extended Data Fig. 5A-C**). These results highlight that bats, including *Myotis*, may have faced greater selective pressures from DNA viruses than from RNA viruses, in contrast to all other mammals.

Evolution of body size & lifespan across nearctic *Myotis*

Beyond their remarkable immune adaptations, bats are exceptional as the longest-lived clade of mammal after correcting for their body size[2,20,80], demonstrating a ~11x range of lifespans within a ~650x range of body sizes[1,80,81]; *Myotis* species in particular exhibit the full dynamic range of bat lifespans within a narrow range of body sizes. While bats have been noted as an exception to the strong allometric scaling (positive correlation with body size) of lifespan otherwise seen across mammals and other metazoans, this exception has not been tested using phylogenetically corrected statistics leveraging well-resolved phylogenies.

To test the hypothesis of non-allometric scaling of lifespan in bats, we modeled the evolution of body size and lifespan independently across a supertree of over 1000 mammals[55] (**Fig. 5A-B; Extended Data Fig. 6A-B**; **Extended Data Table 6**). We generally observed agreement between evolutionary patterns of body size and lifespan in the two simulations, such as in whales (*Cetacea*)[82,83], elephantids (*Proboscidea*)[38,84,85], and primates (**Fig. 5A-B**). However, while only minor changes were observed in their body size, we observed some of the largest and most-rapid changes in lifespan across mammals in bats (**Fig. 5A-B; Extended Data Fig. 6A-B**; **Extended Data Table 6**). These changes are largely independent between species and genera, consistent with the theory of multiple independent increases in lifespan across bats. We used phylogenetically-corrected generalized linear models and ANCOVA to quantify the relationship between body size and lifespan across mammals. While we find that non-bat mammals experience an average 0.159% increase in lifespan per 1% increase in body size, bats experience a 0.223% increase in lifespan years per 1% increase in body size. After phylogenetic correction, however, these rates were not significantly different (**Extended Data Fig. 6C-D**; pANCOVA: p=0.29). In *Myotis*, we saw many of the fastest increases in lifespan relative to their most recent ancestor, including for *Myotis grisescens* (4.15x increase, 100th percentile), *Myotis brandtii* (2.25x increase, 100th percentile), *Myotis lucifugus* (1.56x, 98th percentile), *Myotis myotis* (1.1x increase, 79nd percentile), and the *Myotis* common ancestor (1.26x increase, 92rd percentile) (**Fig. 5B, Extended Data Fig. 6B**). Together these results demonstrate that *Myotis* bats and their recent ancestors have evolved some of the most extreme increases in lifespan among mammals, despite similar allometric lifespan scaling of bats and mammals after phylogenetic correction.

Evolutionary signatures of cancer resistance and pleiotropy with DNA virus adaptations in *Myotis*

Rapid changes in body size and lifespan can have major implications for the evolution of cancer risk and resistance across mammals. The multistage model of carcinogenesis[86–89] posits that cancers arise from mutations accumulated during development and over an organism's life; and that lifetime *cancer risk* scales linearly with body size, and with lifespan as a power-law with exponent 6[88–91]. While these positive correlations have been well-established *within species*[92–97], when comparing *between* species and

accounting for phylogeny and other life history traits, there is only a weak correlation between body size and cancer risk,– and no correlation between lifespan and cancer risk[91,96–99]. This observation, which has been coined *Peto's Paradox*, suggests that species with more cells or longer lifespans have adapted to reduce their cancer risks (i.e. increased cancer resistance) (**Fig. 5C**).

We hypothesized that the extreme changes in lifespan observed throughout the *Myotis* phylogeny should exert a selective pressure on genes associated with cancer processes. Using aBSREL[100] to test for selection at terminal and internal branches within *Myotis*, we found that at FDR<=5%, an average of 5.46% of protein-coding genes had at least one region under positive selection per node (omega >1); in contrast, an average of 20.8% of protein-coding genes per node had all regions with an omega less than 1, suggesting negative selection (**Extended Data Table 7**). Genes under either positive or negative selection were enriched for several pathways in immunity, cancer, and aging, with many sitting at the intersection of multiple processes, suggesting possible pleiotropic selective pressures (**Extended Data Table 7**). Confirming our methods, many of the genes and pathways we identify as under selection in *Myotis* have been previously identified in the literature, such as members of the Cluster of Differentiation (CD) family[26,101], Serpin family[44], insulin signaling pathway[39,102], redox repair[103], and iron storage[104,105] (**Extended Data Fig. 6E; Extended Data Table 7**).

We quantified the contribution of genes under positive selection to pathways associated with the hallmark of cancer[106–108] by measuring the proportion of cancer-associated pathways overrepresented among genes under positive selection throughout the phylogeny (**Fig. 5E**). We observed that most nodes within nearctic *Myotis* were enriched for cancer hallmark pathways among genes under positive selection, especially at the recent ancestors of the longest-lived species (e.g. *M. lucifugus, M. occultus*; **Fig. 5E**). Furthermore, when considering the union of all genes under positive selection in the evolutionary history of each species since their common ancestor, we observed significant enrichments in the representation of cancer-associated pathways in many of the lineages with the greatest cumulative increases in lifespan (*M. lucifugus*, *M. occultus, M. evotis, M. yumanensis;* **Fig. 5F, Extended Data Fig. 6F**). This suggests that selection in genes involved in cancer-related processes occurred concurrently with the recurrent increases in lifespan seen in this clade.

The longest-lived bat in our study, *M. lucifugus*, had an overrepresentation of pathways specifically associated with DNA double-strand break (DSB) repair when looking at both lineage-wide and node-specific enrichments in positive selection using the Reactome database[109] (**Fig. 5G; Extended Data Table 7**). This includes 35 out of 65 genes in the high-fidelity Homologous Recombination Repair pathway, and 21/37 members of the Homology-Directed Repair via Single Strand Annealing (**Fig. 5G; Extended Data Fig. 6E; Extended Data Table 7**). These results suggest that *M. lucifugus* might have an enhanced response to DNA DSBs relative to other bats. To test this hypothesis, we assessed the tolerance of *M. lucifugus* to neocarzinostatin (NCS), a potent radiomimetic agent that induces DNA double-strand breaks[110–112] (**Fig. 5H**), compared to *M. evotis*, three non-*Myotis* bats (*Eidolon helvum, Pteropus rodrigensis,* and *Rousettus lanosus*). At low doses of neocarzinostatin, *M. lucifugus* was the only species tested showing sensitivity to neocarzinostatin after 24 hours, with a drop in viability and concomitant increase in apoptosis. At high doses, *M. lucifugus* had the highest level of apoptosis and the greatest drop in viability of all the bats tested. This is consistent with other long-lived species, including elephants[36,37,113], naked mole rats[46], and bowhead whales[40,114], where longevity are associated with an increased ability to clear out damaged cells.

To better understand the genes that may be driving this difference, we examined RNA expression in *M. lucifugus* cells after 6 and 18 hours of treatment with 100nM NCS. As expected, at 6 hours we observe

up-regulation of genes associated with cell cycle arrest (e.g. *MDM2*, *CDKN1A*) and cell death (e.g. *BAX*), and down-regulation of genes in pathways associated with cell division and growth at 6 hours. At 18 hours, we observe up-regulation of genes in pathways associated with cellular stress response and continued down-regulation of the cell cycle (**Fig. 6A-D, Extended Data Fig. 7A, Extended Data Table 9**). At 6 hours, however, we also observed down-regulation of genes associated with DNA damage repair and synthesis, which together with the up-regulation of *BAX* is consistent with the observed sensitivity to NCS in *M. lucifugus*.

Unexpectedly, however, we observed that the strongest pathway enrichment in our DNA-damage RNA-seq data were genes associated with the innate immune response, including genes in the PI3K/AKT pathway (**Fig. 6C-D, Extended Data Table 9**). We hypothesized that the observed relationship between the unique DNA damage response of *M. lucifugus* may be due to pleiotropy with DNA VIPs and selection in these genes. Indeed, we observed that there was a highly significant enrichment for genes that are differentially expressed after NCS treatment and DNA-only VIPs (p=3.34e-5, **Fig. 6E**; α=0.0245, **Extended Data Fig. 7B**). The genes at the intersection of DNA-only VIPs and NCS response are overrepresented in pathways associated with the cell cycle, senescence, transcription, and DNA damage repair (**Fig. 6F**). To test how selection may have impacted these pleiotropic signatures, we repeated these analyses only considering genes under selection in *Myotis lucifugus*. The intersection between DNA-only VIPs and NCS-DE genes remained highly significant (p=1.88e-3, **Extended Data Fig. 7C**) with only three pathways remaining enriched at FDR<=0.05: Cell Cycle, DNA Damage Repair, and Deubiquination (**Fig. 6G**); DNA-only VIP genes which are not NCS-responsive did not show these signatures (**Extended Data Fig. 7D-G).** Together these results suggest that selection on the innate immune response may drive *agonistic* pleiotropy in aging-associated traits like DNA damage response and cell cycle regulation.

Discussion

Bats are widely known for their long lifespan, and viral tolerance[1,4,13,44,80,97,115–117]. As highly complex and pleiotropic processes, the genes and mechanisms underlying these phenotypes can be challenging to identify, especially for rapidly-evolving phenotypes such as host-pathogen interactions. Here we outline an approach that enables functional comparative biology by generating cell lines from wing punches of wild caught bats for genome assembly, comparative genomics, and functional follow up. Cell lines are generated from minimally-invasive biopsies collected in the field thus avoiding disturbing natural populations. Using this approach, we identify new patterns of adaptation contributing to longevity, cancer resistance, and viral interactions in bats, and demonstrate a unique DNA damage response in primary cells of the long-lived *M. lucifugus.* Given the high density of bat species concentrated at single locations world-wide[118,119] it is feasible to collect wing punches from a large number of individuals across a wide phylogenetic range; these wing punches can be used to generate cell lines and sequencing libraries for reference genomes in a matter of weeks. Furthermore, we find that primary-cell-line-derived genomes are of higher quality than those derived from primary tissues (**Figure S1**). As this approach can generate genomic resources from minimal material gathered via non-lethal sampling, it is also well-suited for conservation genomics and the study of rare or endangered species for which acquiring sufficient amounts of material can be challenging[120–122].

The evolution of body size and lifespan across mammals - and in particular, the rapid evolution of lifespan such as in Yangochiroptera - has major implications for the co-evolution of cancer risk and resistance. While models of body size evolution are well-studied in mammals[11,38,84,123] the evolution of

367 lifespan is less well understood. We find that many extant and ancestral *Myotis* species have experienced
368 some of the fastest rates of change in lifespan seen in mammals, despite minor changes in body size. This
369 altered scaling of longevity in *Myotis* is predicted to have serious consequences for their intrinsic, per-cell
370 cancer risk. Similar to other systems where the evolution of cancer resistance has been largely driven by
371 rapid changes in body size[36–38,45,124,125], the rapid and repeated changes in lifespan across an order of
372 magnitude observed in *Myotis* are hypothesized to result in strong selective pressures on lifetime cancer
373 suppression to avoid premature death by malignancies[80,86,91,126]. This is supported both by recent meta-
374 analyses on cancer risk in vertebrates[96,97,127] demonstrating little to no correlation between neoplasias and
375 either species body size or lifespan; as well as by studies showing weak or no correlation between mutation
376 rates and either species body size or lifespan, respectively[128–130]. For bats, however, there are very limited
377 records for neoplasias in the literature - and only for Yinpterochiropterans[96,97]. The difficulties of maintaining
378 captive colonies of *Myotis* and other Yangochriopterans[131], coupled with their exceptional longevity,
379 necessitates the use of proxy measurements for cancer resistance in these species, such as measuring
380 somatic mutation rates across lifespan and the use of *in vitro* models of carcinogenesis to experimentally
381 test the cancer resistance of long-lived bats[117].

382 Bats are also important models for understanding infectious disease response and immune
383 adaptation because of their unique resistance to viruses and role as zoonotic reservoirs[3,74,132]. Here, we show
384 that while bats have adapted to both DNA and RNA viruses, they demonstrate a remarkable dominance in
385 adaptations to DNA viruses. This is in contrast to humans and other primates, in which adaptation to RNA
386 viruses dominates[50,79]. While bats are known to mount adaptive immune responses to some RNA viruses,
387 this suggests that adaptations in bats' innate and adaptive immune systems, such expansions in *MHC-I* and
388 *APOBEC3*[44], or the loss of the *PYHIN* gene family[49], may be sufficient as a first line of defense to protect
389 against the fitness impacts of some RNA viruses, but not against DNA viruses. This is consistent with
390 previous observations that most zoonoses, including those hosted by bats, are RNA viruses[13] and that bats
391 are more likely than other mammals to asymptomatically harbor RNA viruses, while being more susceptible
392 themselves to other pathogens such as fungi[74]. We also recapitulate and expand on previous results related
393 to positive selection in immune genes and immune gene family expansion, contraction, and loss. In addition,
394 we demonstrate complex patterns of structural variation in immune genes, including a segregating
395 duplication of the Protein Kinase R gene (*PKR*), a major protein involved in the antiviral innate immune
396 system, that has functional relevance in its activity against both DNA and RNA viruses[30]. By resolving
397 individual haplotypes in nine *Myotis* species, we were able to confirm a single duplication event at the origin
398 of *Myotis PKR1* and *PKR2*. We further demonstrate the functional implications of copy number variation in
399 *PKR*, including differences in copy expression and an additive effect on cellular effector functions.

400 Multiple hypotheses have been proposed to connect the unique physiology and ecology of bats with
401 the evolution of remarkable adaptations such as viral infection tolerance, stress tolerance, and exceptional
402 longevity[115]. Hypothesized drivers of disease resistance and longevity evolution in bats include the evolution
403 of flight (e.g. "flight as fever" hypothesis[133], though this hypothesis has recently been critiqued[134]), the
404 disposable soma hypothesis[135]; metabolic state[136]; torpor[1]; and other adaptations to specific
405 environments[101,137–139]. Additionally, many studies have highlighted the intersection of these traits, including
406 a relationship between hibernation and both longevity[1,132] and infectious disease resistance[74,132]. Our results
407 are consistent with an *agonistic* pleiotropy hypothesis, wherein genetic adaptations for many specific traits
408 (e.g. DNA virus innate immunity) may prove beneficial to other seemingly-unrelated traits (e.g. cancer
409 resistance, cellular homeostasis, longevity). Importantly, bats are also the only mammal to harbor active DNA

410 transposons[140,141], the suppression of which may also contribute to signatures of selection in DNA-interacting
411 VIPs.

412 Consistent with the agonistic pleiotropy hypothesis, many of the genes and pathways highlighted in
413 this study have been found to play vital roles across physiological traits in bats and other species. As a core
414 part of the integrated stress response PKR is not only associated with the innate immune response, but also
415 has been identified as a longevity-associated gene in multiple studies[142–144]. Additionally, two genes under
416 selection in nearctic *Myotis* - *FTH1* and *IGFN1* - have been implicated in functional studies as key hibernation
417 genes[145–147], viral interacting proteins[148–151], and as pro-longevity genes[152–154]. Similarly, many DNA VIPs
418 such as *BRCA1/2* and *POLG* are core DNA maintenance genes essential for cancer resistance and
419 longevity[46,155–161]. Such essential genes are generally under increased constraint; however, it is possible that
420 internal pressures, such as DNA transposon activity, and external pressures such as viral infections and
421 other environmental stressors, are shaping the fitness landscape of these essential genes such that novel
422 optimizations become accessible to evolutionary processes[140]. Changes in structural genomic variation also
423 play a crucial role here, such as our findings related to PKR and RNA VIPs in *Myotis*. Many of the overarching
424 pathways we observed under selection, such as inflammation, senescence, and ferroptosis, lie directly at the
425 intersection of aging-related immune processes[44,49,147,152,162–169]. More broadly, our findings on pervasive
426 selection on DNA-only VIPs and the extreme evolution of longevity and cancer risk in other bats support a
427 more general hypothesis that traits such as cancer risk, cellular homeostasis, and antiviral response have
428 evolved in tandem due to pleiotropic selection at coinciding points in bats' evolutionary history. Further work
429 leveraging model systems such as *Myotis* for functional evolutionary genomics is necessary to disambiguate
430 the underlying selective pressures driving these functional genetic changes in bats and beyond.

431 Acknowledgements

432 PacBio HiFi sequencing was done by the DNA Technologies and Expression Analysis Cores at the UC Davis
433 Genome Center (NIH SIG 1S10OD010786-01). Analyses were performed using the High Performance
434 Computing (HPC) resources at the University of Arizona (supported by the University of Arizona TRIF, UITS,
435 and Research, Innovation, and Impact (RII); maintained by the UArizona Research Technologies
436 department); the Savio computational cluster resource provided by the Berkeley Research Computing
437 program at the University of California, Berkeley (supported by the UC Berkeley Chancellor, Vice Chancellor
438 for Research, and Chief Information Officer); and the Vermont Advanced Computing Core at . We thank the
439 members of the LP2L team (CIRI) for helpful discussions.

440 MEL was funded by NSF PRFB #2010884, and a Dovetail Tree of Life Grant. JMV was funded by NSF PRFB
441 #2109915, NIH NIA T32AG000266, and NIA 1K99AG088361. DE was funded by NIH NIGMS MIRA grant
442 5R35GM142677. PHS was funded by NIH NIGMS R35GM142916 and by the Vallee Scholars Award. LE
443 was funded by a grant from the Agence Nationale de la Recherche (ANR, #ANR-202-CE15-0020-01 to LE)
444 and CNRS MITI These Internationale (to M.S. and L.E.). SP is funded by the ANR (ANR-21-CE35-0018-01)
445 and by the Interdisciplinary Thematic Institute IMCbio+ supported by IdEx Unistra (ANR-10-IDEX-0002), by
446 SFRI-STRAT'US project (ANR-20-SFRI-0012) and EUR IMCBio (IMCBio ANR-17-EURE-0023) under the
447 framework of the French Investments for the Future Program. LE and DE were further funded by a grant
448 from the Joint Call for Proposals between the CNRS and the University of Arizona (International Research
449 Center, IRC, 2021-2024). LE, DE, PHS and SP were further funded by the International Research Project
450 (IRP) RAPIDvBAT from the CNRS, the University of Arizona and the University of California, Berkeley. LG

was funded by a postdoctoral fellowship from the Fondation pour la Recherche Médicale (FRM, #SPF202209015746).

Image attributions for the bat photos featured in Fig. 1: J. Scott Altenbach (*M. thysanodes*); M. Elise Lauterbur (*M. occultus, M. velifer*); U.S. National Park Service (*M. auriculus*); Frank Carey (*M. californicus*); Michael Durham (*M. evotis*); J. N. Stuart (*M. volans*); and SMBishop & the Wikimedia Foundation (*M. lucifugus*).

Author Contributions:

Conceptualization, J.M.V., M.E.L., D.E., P.H.S., L.E., D.F., M.B.; Methodology, J.M.V., M.E.L., D.E., P.H.S., L.E., G.G.S.; Software, J.M.V., M.E.L., D.E., P.H.S., L.E., T.M.L.; Validation, J.M.V., M.E.L., D.E., P.H.S., L.E., J.P.V.M.; Formal Analysis, J.M.V., M.E.L., D.E., P.H.S., L.E., S.M., A.L.C., D.M., S.V.; Investigation, J.M.V., M.E.L., S.M., M.B., D.F., G.G.S., L.G., Z.R.H., M.H., W.K., T.M.L., A.L.C., C.L. S.M., D.M., S.L., J.L., C.R., S.L.R.C., M.S., K.S., W.T., J.D.T., S.V., R.M., M.B., J.P.V.M., S.P., L.E., D.E., P.H.S.; Resources, J.M.V., M.E.L., D.E., P.H.S., L.E., M.B., D.F., G.G.S., L.G., Z.R.H., M.H., W.K., T.M.L., A.L.C., S.M., D.M., S.L., J.L., C.R., S.L.R.C., M.S., K.S., W.T., J.D.T., S.V., R.M., M.B.; Data Curation, J.M.V., M.E.L., S.M., M.B., D.F., G.G.S., L.G., Z.R.H., M.H., W.K., T.M.L., A.L.C., S.M., D.M., S.L., J.L., C.R., S.L.R.C., M.S., K.S., W.T., J.D.T., S.V., R.M., M.B., J.P.V.M., S.P., L.E., D.E., P.H.S.; Writing - Original Draft, J.M.V., M.E.L., D.E., P.H.S., L.E., S.M., J.L.; Writing - Review & Editing, J.M.V., M.E.L., S.M., M.B., D.F., G.G.S., L.G., Z.R.H., M.H., W.K., T.M.L., A.L.C., S.M., D.M., S.L., J.L., C.R., S.L.R.C., M.S., K.S., W.T., J.D.T., S.V., R.M., M.B., J.P.V.M., S.P., L.E., D.E., P.H.S.; Visualization, J.M.V., M.E.L., D.E., P.H.S., L.E., S.M., A.L.C.; Supervision, J.M.V., M.E.L., D.E., P.H.S., L.E.; Project Administration, J.M.V., M.E.L., D.E., P.H.S., L.E.; Funding Acquisition, J.M.V., M.E.L., D.E., P.H.S., L.E.

Declaration of Interests:

The authors declare no competing interests.

References

1. Wilkinson, G.S., and Adams, D.M. (2019). Recurrent Evolution of Extreme Longevity in Bats. Biol. Lett. *15*, 20180860. https://doi.org/10.1098/rsbl.2018.0860.

2. Austad, S.N., and Fischer, K.E. (1991). Mammalian Aging, Metabolism, and Ecology: Evidence from the Bats and Marsupials. J. Gerontol. *46*, B47–B53. https://doi.org/10.1093/geronj/46.2.b47.

3. Guth, S., Mollentze, N., Renault, K., Streicker, D.G., Visher, E., Boots, M., and Brook, C.E. (2022). Bats host the most virulent-but not the most dangerous-zoonotic viruses. Proc. Natl. Acad. Sci. U. S. A. *119*, e2113628119. https://doi.org/10.1073/pnas.2113628119.

4. Irving, A.T., Ahn, M., Goh, G., Anderson, D.E., and Wang, L.-F. (2021). Lessons from the host defences of bats, a unique viral reservoir. Nature *589*, 363–370. https://doi.org/10.1038/s41586-020-03128-0.

5. Cooper, L.N., Ansari, M.Y., Capshaw, G., Galazyuk, A., Lauer, A.M., Moss, C.F., Sears, K.E., Stewart, M., Teeling, E.C., Wilkinson, G.S., et al. (2024). Bats as instructive animal models for studying longevity and aging. Ann. N. Y. Acad. Sci. *1541*, 10–23. https://doi.org/10.1111/nyas.15233.

6. Wilson, D.E., and Reeder, D.M. (2005). Mammal Species of the World: A Taxonomic and Geographic Reference (JHU Press).

7. Simmons, N.B., and Cirranello, A.L. Bat Species of the World: A Taxonomic and Geographic Database. https://batnames.org/.

8. Teeling, E.C., Hedges, S.B., and Kumar, S. (2009). Bats (Chiroptera). The timetree of life, 499–503.

9. Rietbergen, T.B., Ostende, L.W. van den H., Aase, A., Jones, M.F., Medeiros, E.D., and Simmons, N.B. (2023). The Oldest Known Bat Skeletons and Their Implications for Eocene Chiropteran Diversification. PLoS One *18*, e0283505. https://doi.org/10.1371/journal.pone.0283505.

10. Kumar, S., Stecher, G., Suleski, M., and Hedges, S.B. (2017). TimeTree: A Resource for Timelines, Timetrees, and Divergence Times. Mol. Biol. Evol. *34*, 1812–1819. https://doi.org/10.1093/molbev/msx116.

11. Moyers Arévalo, R.L., Amador, L.I., Almeida, F.C., and Giannini, N.P. (2020). Evolution of Body Mass in Bats: Insights from a Large Supermatrix Phylogeny. J. Mamm. Evol. *27*, 123–138. https://doi.org/10.1007/s10914-018-9447-8.

12. Datzmann, T., von Helversen, O., and Mayer, F. (2010). Evolution of Nectarivory in Phyllostomid Bats (Phyllostomidae Gray, 1825, Chiroptera: Mammalia). BMC Evol. Biol. *10*, 165. https://doi.org/10.1186/1471-2148-10-165.

13. Hayman, D.T.S., Bowen, R.A., Cryan, P.M., McCracken, G.F., O'Shea, T.J., Peel, A.J., Gilbert, A., Webb, C.T., and Wood, J.L.N. (2013). Ecology of zoonotic infectious diseases in bats: current knowledge and future directions. Zoonoses Public Health *60*, 2–21. https://doi.org/10.1111/zph.12000.

14. Camacho, J., Bernal-Rivera, A., Peña, V., Morales-Sosa, P., Robb, S.M.C., Russell, J., Yi, K., Wang, Y., Tsuchiya, D., Murillo-García, O.E., et al. (2023). Sugar assimilation underlying dietary evolution of Neotropical bats. Nat. Ecol. Evol. *8*, 1735–1750. https://doi.org/10.1038/s41559-024-02485-7.

15. Morales, A.E., Ruedi, M., Field, K., and Carstens, B.C. (2019). Diversification rates have no effect on the convergent evolution of foraging strategies in the most speciose genus of bats, Myotis. Evolution *73*, 2263–2280. https://doi.org/10.1111/evo.13849.

16. Gunnell, G.F., Smith, R., and Smith, T. (2017). 33 Million Year Old Myotis (Chiroptera, Vespertilionidae) and the Rapid Global Radiation of Modern Bats. PLoS One *12*, e0172621. https://doi.org/10.1371/journal.pone.0172621.

17. Ruedi, M., Stadelmann, B., Gager, Y., Douzery, E.J.P., Francis, C.M., Lin, L.-K., Guillén-Servent, A., and Cibois, A. (2013). Molecular Phylogenetic Reconstructions Identify East Asia as the Cradle for the Evolution of the Cosmopolitan Genus Myotis (Mammalia, Chiroptera). Mol. Phylogenet. Evol. *69*, 437–449. https://doi.org/10.1016/j.ympev.2013.08.011.

18. Tacutu, R., Craig, T., Budovsky, A., Wuttke, D., Lehmann, G., Taranukha, D., Costa, J., Fraifeld, V.E., and de Magalhães, J.P. (2013). Human Ageing Genomic Resources: Integrated Databases and Tools for the Biology and Genetics of Ageing. Nucleic Acids Res. *41*, D1027–D1033. https://doi.org/10.1093/nar/gks1155.

19. Jones, K.E., Bielby, J., Cardillo, M., Fritz, S.A., O'Dell, J., Orme, C.D.L., Safi, K., Sechrest, W., Boakes, E.H., Carbone, C., et al. (2009). PanTHERIA: A Species-Level Database of Life History, Ecology, and Geography of Extant and Recently Extinct Mammals. Ecology *90*, 2648–2648. https://doi.org/10.1890/08-1494.1.

20. Austad, S.N. (2010). Methusaleh's Zoo: How Nature Provides Us with Clues for Extending Human Health Span. J. Comp. Pathol. *142*, S10–S21. https://doi.org/10.1016/j.jcpa.2009.10.024.

21. Podlutsky, A.J., Khritankov, A.M., Ovodov, N.D., and Austad, S.N. (2005). A new field record for bat longevity. J. Gerontol. A Biol. Sci. Med. Sci. *60*, 1366–1368. https://doi.org/10.1093/gerona/60.11.1366.

22. Wilson, D.E., and Tyson, E.L. (1970). Longevity Records for Artibeus Jamaicensis and Myotis Nigricans. J. Mammal. *51*, 203. https://doi.org/10.2307/1378570.

23. Stadelmann, B., Lin, L.-K., Kunz, T.H., and Ruedi, M. (2007). Molecular Phylogeny of New World \emphMyotis (Chiroptera, Vespertilionidae) Inferred from Mitochondrial and Nuclear DNA Genes. Mol. Phylogenet. Evol. *43*, 32–48. https://doi.org/10.1016/j.ympev.2006.06.019.

24. Agnarsson, I., Zambrana-Torrelio, C.M., Flores-Saldana, N.P., and May-Collado, L.J. (2011). A Time-Calibrated Species-Level Phylogeny of Bats (Chiroptera, Mammalia). PLoS Curr. *3*, RRN1212. https://doi.org/10.1371/currents.RRN1212.

25. Armero, A., Li, R., Bienes, K.M., Chen, X., Li, J., Xu, S., Chen, Y., Hughes, A.C., Berthet, N., and Wong, G. (2022). Myotis Fimbriatus Virome, a Window to Virus Diversity and Evolution in the Genus Myotis. Viruses *14*, 1899. https://doi.org/10.3390/v14091899.

26. He, X., Korytář, T., Zhu, Y., Pikula, J., Bandouchova, H., Zukal, J., and Köllner, B. (2014). Establishment of Myotis Myotis Cell Lines - Model for Investigation of Host-Pathogen Interaction in a Natural Host for Emerging Viruses. PLoS One *9*, e109795. https://doi.org/10.1371/journal.pone.0109795.

27. Seltmann, A., Troxell, S.A., Schad, J., Fritze, M., Bailey, L.D., Voigt, C.C., and Czirják, G.Á. (2022). Differences in Acute Phase Response to Bacterial, Fungal and Viral Antigens in Greater Mouse-Eared Bats (Myotis Myotis). Sci. Rep. *12*, 15259. https://doi.org/10.1038/s41598-022-18240-6.

28. Hayward, J.A., Tachedjian, M., Johnson, A., Irving, A.T., Gordon, T.B., Cui, J., Nicolas, A., Smith, I., Boyd, V., Marsh, G.A., et al. (2022). Unique Evolution of Antiviral Tetherin in Bats. J. Virol. *96*, e0115222. https://doi.org/10.1128/jvi.01152-22.

29. Fernandes, A.P., Águeda-Pinto, A., Pinheiro, A., Rebelo, H., and Esteves, P.J. (2022). Evolution of TRIM5 and TRIM22 in Bats Reveals a Complex Duplication Process. Viruses *14*. https://doi.org/10.3390/v14020345.

30. Jacquet, S., Culbertson, M., Zhang, C., El Filali, A., De La Myre Mory, C., Pons, J.-B., Filippi-Codaccioni, O., Lauterbur, M.E., Ngoubangoye, B., Duhayer, J., et al. (2022). Adaptive duplication and genetic diversification of protein kinase R contribute to the specificity of bat-

569 virus interactions. Sci Adv *8*, eadd7540. https://doi.org/10.1126/sciadv.add7540.

570 31. Jacquet, S., Pontier, D., and Etienne, L. (2020). Rapid Evolution of HERC6 and Duplication of
571 a Chimeric HERC5/6 Gene in Rodents and Bats Suggest an Overlooked Role of HERCs in
572 Mammalian Immunity. Front. Immunol. *11*, 605270.
573 https://doi.org/10.3389/fimmu.2020.605270.

574 32. Chomel, B., Stuckey, M., Boulouis, H., and Aguilar Setién, Á. (2014). Bat-Related Zoonoses.
575 Zoonoses - Infections Affecting Humans and Animals, 697–714. https://doi.org/10.1007/978-
576 94-017-9457-2_28.

577 33. Williams, E.P., Spruill-Harrell, B.M., Taylor, M.K., Lee, J., Nywening, A.V., Yang, Z., Nichols,
578 J.H., Camp, J.V., Owen, R.D., and Jonsson, C.B. (2021). Common themes in zoonotic spillover
579 and disease emergence: Lessons learned from bat- and rodent-borne RNA viruses. Viruses
580 *13*, 1509. https://doi.org/10.3390/v13081509.

581 34. Mollentze, N., and Streicker, D.G. (2020). Viral zoonotic risk is homogenous among taxonomic
582 orders of mammalian and avian reservoir hosts. Proc. Natl. Acad. Sci. U. S. A. *117*, 9423–
583 9430. https://doi.org/10.1073/pnas.1919176117.

584 35. Kolora, S.R.R., Owens, G.L., Vazquez, J.M., Stubbs, A., Chatla, K., Jainese, C., Seeto, K.,
585 McCrea, M., Sandel, M.W., Vianna, J.A., et al. (2021). Origins and Evolution of Extreme Life
586 Span in Pacific Ocean Rockfishes. Science *374*, 842–847.
587 https://doi.org/10.1126/science.abg5332.

588 36. Sulak, M., Fong, L., Mika, K., Chigurupati, S., Yon, L., Mongan, N.P., Emes, R.D., and Lynch,
589 V.J. (2016). Correction: TP53 copy number expansion is associated with the evolution of
590 increased body size and an enhanced DNA damage response in elephants. Elife *5*.
591 https://doi.org/10.7554/eLife.24307.

592 37. Vazquez, J.M., Sulak, M., Chigurupati, S., and Lynch, V.J. (2018). A Zombie LIF Gene in
593 Elephants Is Upregulated by TP53 to Induce Apoptosis in Response to DNA Damage. Cell
594 Rep. *24*, 1765–1776. https://doi.org/10.1016/j.celrep.2018.07.042.

595 38. Vazquez, J.M., and Lynch, V.J. (2021). Pervasive duplication of tumor suppressors in
596 Afrotherians during the evolution of large bodies and reduced cancer risk. Elife *10*, e65041.
597 https://doi.org/10.7554/eLife.65041.

598 39. Davies, K.T.J., Tsagkogeorga, G., Bennett, N.C., Dávalos, L.M., Faulkes, C.G., and Rossiter,
599 S.J. (2014). Molecular Evolution of Growth Hormone and Insulin-like Growth Factor 1
600 Receptors in Long-Lived, Small-Bodied Mammals. Gene *549*, 228–236.
601 https://doi.org/10.1016/j.gene.2014.07.061.

602 40. Vazquez, J.M., Kraft, M., and Lynch, V.J. (2022). A CDKN2C retroduplication in Bowhead
603 whales is associated with the evolution of extremely long lifespans and alerted cell cycle
604 dynamics. bioRxiv, 2022.09.07.506958. https://doi.org/10.1101/2022.09.07.506958.

605 41. Foote, A.D., Liu, Y., Thomas, G.W.C., Vinař, T., Alföldi, J., Deng, J., Dugan, S., van Elk, C.E.,
606 Hunter, M.E., Joshi, V., et al. (2015). Convergent evolution of the genomes of marine
607 mammals. Nat. Genet. *47*, 272–275. https://doi.org/10.1038/ng.3198.

608 42. Huang, Z., Jiang, C., Gu, J., Uvizl, M., Power, S., Douglas, D., and Kacprzyk, J. (2023).
609 Duplications of Human Longevity-Associated Genes Across Placental Mammals. Genome Biol.
610 Evol. *15*. https://doi.org/10.1093/gbe/evad186.

611 43. Li, S., Vazquez, J.M., and Sudmant, P.H. (2023). The evolution of aging and lifespan. Trends
612 Genet. *39*, 830–843. https://doi.org/10.1016/j.tig.2023.08.005.

613 44. Jebb, D., Huang, Z., Pippel, M., Hughes, G.M., Lavrichenko, K., Devanna, P., Winkler, S.,
614 Jermiin, L.S., Skirmuntt, E.C., Katzourakis, A., et al. (2020). Six reference-quality genomes
615 reveal evolution of bat adaptations. Nature *583*, 578–584. https://doi.org/10.1038/s41586-020-
616 2486-3.

617 45. Glaberman, S., Bulls, S.E., Vazquez, J.M., Chiari, Y., and Lynch, V.J. (2021). Concurrent
618 evolution of antiaging gene duplications and cellular phenotypes in long-lived turtles. Genome
619 Biol. Evol. *13*, evab244. https://doi.org/10.1093/gbe/evab244.

620 46. MacRae, S.L., Croken, M.M., Calder, R.B., Aliper, A., Milholland, B., White, R.R., Zhavoronkov,
621 A., Gladyshev, V.N., Seluanov, A., Gorbunova, V., et al. (2015). DNA Repair in Species with
622 Extreme Lifespan Differences. Aging *7*, 1171–1184. https://doi.org/10.18632/aging.100866.

623 47. Baines, C., Meitern, R., Kreitsberg, R., and Sepp, T. (2022). Comparative study of the evolution
624 of cancer gene duplications across fish. Evol. Appl. *15*, 1834–1845.
625 https://doi.org/10.1111/eva.13481.

626 48. López-Otín, C., Blasco, M.A., Partridge, L., Serrano, M., and Kroemer, G. (2013). The
627 Hallmarks of Aging. Cell *153*, 1194–1217. https://doi.org/10.1016/j.cell.2013.05.039.

628 49. Moreno Santillán, D.D., Lama, T.M., Gutierrez Guerrero, Y.T., Brown, A.M., Donat, P., Zhao,
629 H., Rossiter, S.J., Yohe, L.R., Potter, J.H., Teeling, E.C., et al. (2021). Large-scale genome
630 sampling reveals unique immunity and metabolic adaptations in bats. Mol. Ecol. *30*, 6449–
631 6467. https://doi.org/10.1111/mec.16027.

632 50. Enard, D., and Petrov, D.A. (2020). Ancient RNA virus epidemics through the lens of recent
633 adaptation in human genomes. Philos. Trans. R. Soc. Lond. B Biol. Sci. *375*, 20190575.
634 https://doi.org/10.1098/rstb.2019.0575.

635 51. Sotero-Caio, C.G., Baker, R.J., and Volleth, M. (2017). Chromosomal evolution in Chiroptera.
636 Genes (Basel) *8*. https://doi.org/10.3390/genes8100272.

637 52. Simão, F.A., Waterhouse, R.M., Ioannidis, P., Kriventseva, E.V., and Zdobnov, E.M. (2015).
638 BUSCO: assessing genome assembly and annotation completeness with single-copy
639 orthologs. Bioinformatics *31*, 3210–3212. https://doi.org/10.1093/bioinformatics/btv351.

640 53. Manni, M., Berkeley, M.R., Seppey, M., and Zdobnov, E.M. (2021). BUSCO: assessing
641 genomic data quality and beyond. Current Protocols *1*.

642 54. Amador, L.I., Moyers Arévalo, R.L., Almeida, F.C., Catalano, S.A., and Giannini, N.P. (2018).
643 Bat Systematics in the Light of Unconstrained Analyses of a Comprehensive Molecular
644 Supermatrix. J. Mamm. Evol. *25*, 37–70. https://doi.org/10.1007/s10914-016-9363-8.

645 55. Upham, N.S., Esselstyn, J.A., and Jetz, W. (2019). Inferring the mammal tree: Species-level
646 sets of phylogenies for questions in ecology, evolution, and conservation. PLoS Biol. *17*,
647 e3000494. https://doi.org/10.1371/journal.pbio.3000494.

648 56. Korstian, J.M., Paulat, N.S., Platt, R.N., Stevens, R.D., and Ray, D.A. (2022). SINE-Based
649 Phylogenomics Reveal Extensive Introgression and Incomplete Lineage Sorting in Myotis.
650 Genes *13*, 399. https://doi.org/10.3390/genes13030399.

651 57. Foley, N.M., Harris, A.J., Bredemeyer, K.R., Ruedi, M., Puechmaille, S.J., Teeling, E.C.,
652 Criscitiello, M.F., and Murphy, W.J. (2024). Karyotypic stasis and swarming influenced the
653 evolution of viral tolerance in a species-rich bat radiation. Cell Genom *4*, 100482.
654 https://doi.org/10.1016/j.xgen.2023.100482.

655 58. Foley, N.M., Mason, V.C., Harris, A.J., Bredemeyer, K.R., Damas, J., Lewin, H.A., Eizirik, E.,
656 Gatesy, J., Karlsson, E.K., Lindblad-Toh, K., et al. (2023). A genomic timescale for placental
657 mammal evolution. Science *380*, eabl8189. https://doi.org/10.1126/science.abl8189.

658 59. Volleth, M. (2012). Variations on a theme: Karyotype comparison in Eurasian Myotis species
659 and implications for phylogeny. Vespertilio *16*, 329–350.

660 60. McBee, K. (1986). Standard karyology of nine species of vespertilionid bats (Chiroptera:
661 Vespertilionidae) from Thailand. Annals of Carnegie Museum *55*, 95–116.

662 61. Bickham, J.W., McBee, K., and Schlitter, D.A. (1986). Chromosomal variation among seven
663 species of Myotis (Chiroptera: Vespertilionidae). J. Mammal. *67*, 746–750.
664 https://doi.org/10.2307/1381139.

665 62. Zhang, W.D. (1984). A study on karyotype of Myotis chinensis and M. laniger Peter. J Anhui
666 Normal Univ *7*, 42–47.

667 63. Zima, J. (1985). Synopsis of karyotypes of vespertilionid bats (Mammalia: Chiroptera). Acta
668 Univ. Carol. Biol *1981*, 311–329.

669 64. O'Brien, S.J., Menninger, J.C., and Nash, W.G. (2006). Atlas of Mammalian Chromosomes
670 (John Wiley & Sons).

671 65. Goel, M., Sun, H., Jiao, W.-B., and Schneeberger, K. (2019). SyRI: finding genomic
672 rearrangements and local sequence differences from whole-genome assemblies. Genome Biol.
673 *20*, 277. https://doi.org/10.1186/s13059-019-1911-0.

674 66. de Sotero-Caio, C.G., Cabral-de-Mello, D.C., Calixto, M. da S., Valente, G.T., Martins, C.,
675 Loreto, V., de Souza, M.J., and Santos, N. (2017). Centromeric enrichment of LINE-1
676 retrotransposons and its significance for the chromosome evolution of Phyllostomid bats.
677 Chromosome Res. *25*, 313–325. https://doi.org/10.1007/s10577-017-9565-9.

678 67. Morel, B., Kozlov, A.M., Stamatakis, A., and Szöllősi, G.J. (2020). GeneRax: A Tool for
679 Species-Tree-Aware Maximum Likelihood-Based Gene Family Tree Inference under Gene
680 Duplication, Transfer, and Loss. Mol. Biol. Evol. *37*, 2763–2774.
681 https://doi.org/10.1093/molbev/msaa141.

682 68. Kaufman, R.J. (1999). Double-stranded RNA-activated protein kinase mediates virus-induced
683 apoptosis: a new role for an old actor. Proc. Natl. Acad. Sci. U. S. A. *96*, 11693–11695.
684 https://doi.org/10.1073/pnas.96.21.11693.

685 69. García, M.A., Gil, J., Ventoso, I., Guerra, S., Domingo, E., Rivas, C., and Esteban, M. (2006).
686 Impact of protein kinase PKR in cell biology: from antiviral to antiproliferative action. Microbiol.
687 Mol. Biol. Rev. *70*, 1032–1060. https://doi.org/10.1128/MMBR.00027-06.

688 70. Ostertag, D., Hoblitzell-Ostertag, T.M., and Perrault, J. (2007). Overproduction of double-
689 stranded RNA in vesicular stomatitis virus-infected cells activates a constitutive cell-type-
690 specific antiviral response. J. Virol. *81*, 503–513. https://doi.org/10.1128/JVI.01218-06.

691 71. Enard, D., Cai, L., Gwennap, C., and Petrov, D.A. (2016). Viruses are a dominant driver of
692 protein adaptation in mammals. Elife *5*. https://doi.org/10.7554/eLife.12469.

693 72. Murrell, B., Weaver, S., Smith, M.D., Wertheim, J.O., Murrell, S., Aylward, A., Eren, K., Pollner,
694 T., Martin, D.P., Smith, D.M., et al. (2015). Gene-wide identification of episodic selection. Mol.
695 Biol. Evol. *32*, 1365–1371. https://doi.org/10.1093/molbev/msv035.

696 73. Souilmi, Y., Lauterbur, M.E., Tobler, R., Huber, C.D., Johar, A.S., Moradi, S.V., Johnston,
697 W.A., Krogan, N.J., Alexandrov, K., and Enard, D. (2021). An ancient viral epidemic involving
698 host coronavirus interacting genes more than 20,000 years ago in East Asia. Curr. Biol. *31*,
699 3704. https://doi.org/10.1016/j.cub.2021.07.052.

700 74. Brook, C.E., and Dobson, A.P. (2015). Bats as "special" reservoirs for emerging zoonotic
701 pathogens. Trends Microbiol. *23*, 172–180. https://doi.org/10.1016/j.tim.2014.12.004.

702 75. Kondrashov, F.A. (2011). Gene Dosage and Duplication. In Evolution after Gene Duplication,
703 K. Dittmar and D. Liberles, eds. (John Wiley & Sons), pp. 57–76.

704 76. Kondrashov, F.A., Rogozin, I.B., Wolf, Y.I., and Koonin, E.V. (2002). Selection in the evolution
705 of gene duplications. Genome Biol. *3*, RESEARCH0008. https://doi.org/10.1186/gb-2002-3-2-
706 research0008.

707 77. Rastogi, S., and Liberles, D.A. (2005). Subfunctionalization of duplicated genes as a transition
708 state to neofunctionalization. BMC Evol. Biol. *5*, 28. https://doi.org/10.1186/1471-2148-5-28.

709 78. Assis, R., and Bachtrog, D. (2013). Neofunctionalization of young duplicate genes in
710 Drosophila. Proc. Natl. Acad. Sci. U. S. A. *110*, 17409–17414.
711 https://doi.org/10.1073/pnas.1313759110.

712 79. Enard, D., and Petrov, D.A. (2018). Evidence that RNA Viruses Drove Adaptive Introgression
713 between Neanderthals and Modern Humans. Cell *175*, 360–371.e13.
714 https://doi.org/10.1016/j.cell.2018.08.034.

715 80. Brunet-Rossinni, A.K., and Austad, S.N. (2004). Ageing studies on bats: a review.
716 Biogerontology *5*, 211–222. https://doi.org/10.1023/B:BGEN.0000038022.65024.d8.

717 81. Wilkinson, G.S., and South, J.M. (2002). Life History, Ecology and Longevity in Bats. Aging
718 Cell *1*, 124–131. https://doi.org/10.1046/j.1474-9728.2002.00020.x.

719 82. Pyenson, N.D., and Sponberg, S.N. (2011). Reconstructing body size in extinct crown Cetacea
720 (neoceti) using allometry, phylogenetic methods and tests from the fossil record. J. Mamm.
721 Evol. *18*, 269–288. https://doi.org/10.1007/s10914-011-9170-1.

722 83. Montgomery, S.H., Geisler, J.H., McGowen, M.R., Fox, C., Marino, L., and Gatesy, J. (2013).
723 The evolutionary history of cetacean brain and body size: Cetacean brain evolution. Evolution
724 *67*, 3339–3353. https://doi.org/10.1111/evo.12197.

725 84. Puttick, M.N., and Thomas, G.H. (2015). Fossils and living taxa agree on patterns of body
726 mass evolution: a case study with Afrotheria. Proc. Biol. Sci. *282*, 20152023.
727 https://doi.org/10.1098/rspb.2015.2023.

728 85. Sulak, M., Fong, L., Mika, K., Chigurupati, S., Yon, L., Mongan, N.P., Emes, R.D., and Lynch,
729 V.J. (2016). TP53 copy number expansion is associated with the evolution of increased body
730 size and an enhanced DNA damage response in elephants. Elife *5*.

731 https://doi.org/10.7554/elife.11994.

732 86. Nunney, L. (2016). Commentary: The multistage model of carcinogenesis, Peto's paradox and
733 evolution. Int. J. Epidemiol. *45*, 649–653. https://doi.org/10.1093/ije/dyv201.

734 87. Nunney, L. (1999). Lineage selection and the evolution of multistage carcinogenesis. Proc.
735 Biol. Sci. *266*, 493–498. https://doi.org/10.1098/rspb.1999.0664.

736 88. Armitage, P. (1985). Multistage Models of Carcinogenesis. Environ. Health Perspect. *63*, 195–
737 201. https://doi.org/10.1289/ehp.8563195.

738 89. Armitage, P., and Doll, R. (2004). The Age Distribution of Cancer and a Multi-Stage Theory of
739 Carcinogenesis. Br. J. Cancer *91*, 6602297. https://doi.org/10.1038/sj.bjc.6602297.

740 90. Peto, R., Roe, F.J., Lee, P.N., Levy, L., and Clack, J. (1975). Cancer and ageing in mice and
741 men. Br. J. Cancer *32*, 411–426. https://doi.org/10.1038/bjc.1975.242.

742 91. Peto, R. (2015). Quantitative Implications of the Approximate Irrelevance of Mammalian Body
743 Size and Lifespan to Lifelong Cancer Risk. Philos. Trans. R. Soc. Lond. B Biol. Sci. *370*,
744 20150198. https://doi.org/10.1098/rstb.2015.0198.

745 92. Siegel, R.L., Miller, K.D., and Jemal, A. (2018). Cancer Statistics, 2018. CA Cancer J. Clin. *68*,
746 7–30. https://doi.org/10.3322/caac.21442.

747 93. Garner, W.B., Smith, B.D., Ludmir, E.B., Wakefield, D.V., Shabason, J., Williams, G.R., Martin,
748 M.Y., Wang, Y., Ballo, M.T., and VanderWalde, N.A. (2023). Predicting Future Cancer
749 Incidence by Age, Race, Ethnicity, and Sex. J. Geriatr. Oncol. *14*, 101393.
750 https://doi.org/10.1016/j.jgo.2022.10.008.

751 94. Nunney, L. (2024). The effect of body size and inbreeding on cancer mortality in breeds of the
752 domestic dog: a test of the multi-stage model of carcinogenesis. R. Soc. Open Sci. *11*, 231356.
753 https://doi.org/10.1098/rsos.231356.

754 95. Kent, M.S., Karchemskiy, S., Culp, W.T.N., Lejeune, A.T., Pesavento, P.A., Toedebusch, C.,
755 Brady, R., and Rebhun, R. (2022). Longevity and mortality in cats: A single institution necropsy
756 study of 3108 cases (1989-2019). PLoS One *17*, e0278199.
757 https://doi.org/10.1371/journal.pone.0278199.

758 96. Compton, Z.T., Harris, V., Mellon, W., Rupp, S., Mallo, D., Kapsetaki, S.E., Wilmot, M.,
759 Kennington, R., Noble, K., Baciu, C., et al. (2023). Cancer prevalence across vertebrates. Res.
760 Sq. https://doi.org/10.21203/rs.3.rs-3117313/v1.

761 97. Vincze, O., Colchero, F., Lemaître, J.-F., Conde, D.A., Pavard, S., Bieuville, M., Urrutia, A.O.,
762 Ujvari, B., Boddy, A.M., Maley, C.C., et al. (2022). Cancer risk across mammals. Nature *601*,
763 263–267. https://doi.org/10.1038/s41586-021-04224-5.

764 98. Nunney, L. (2018). Size Matters: Height, Cell Number and a Person's Risk of Cancer. Proc. R.
765 Soc. B *285*, 20181743. https://doi.org/10.1098/rspb.2018.1743.

766 99. Caulin, A.F., and Maley, C.C. (2011). Peto's Paradox: evolution's prescription for cancer
767 prevention. Trends Ecol. Evol. *26*, 175–182. https://doi.org/10.1016/j.tree.2011.01.002.

768 100. Smith, M.D., Wertheim, J.O., Weaver, S., Murrell, B., Scheffler, K., and Kosakovsky Pond, S.L.
769 (2015). Less is more: an adaptive branch-site random effects model for efficient detection of

770 episodic diversifying selection. Mol. Biol. Evol. *32*, 1342–1353.
771 https://doi.org/10.1093/molbev/msv022.

772 101. Pei, G., Balkema-Buschmann, A., and Dorhoi, A. (2024). Disease tolerance as immune
773 defense strategy in bats: One size fits all? PLoS Pathog. *20*, e1012471.
774 https://doi.org/10.1371/journal.ppat.1012471.

775 102. Seim, I., Fang, X., Xiong, Z., Lobanov, A.V., Huang, Z., Ma, S., Feng, Y., Turanov, A.A., Zhu,
776 Y., Lenz, T.L., et al. (2013). Genome Analysis Reveals Insights into Physiology and Longevity
777 of the Brandt's Bat Myotis Brandtii. Nat. Commun. *4*, 2212.
778 https://doi.org/10.1038/ncomms3212.

779 103. Matsuda, Y., and Makino, T. (2024). Comparative genomics reveals convergent signals
780 associated with the high metabolism and longevity in birds and bats. Proc. Biol. Sci. *291*,
781 20241068. https://doi.org/10.1098/rspb.2024.1068.

782 104. Blumer, M., Brown, T., Freitas, M.B., Destro, A.L., Oliveira, J.A., Morales, A.E., Schell, T.,
783 Greve, C., Pippel, M., Jebb, D., et al. (2022). Gene losses in the common vampire bat
784 illuminate molecular adaptations to blood feeding. Sci. Adv. *8*, eabm6494.
785 https://doi.org/10.1126/sciadv.abm6494.

786 105. Morales, A.E., Burbrink, F.T., Segall, M., Meza, M., Munegowda, C., Webala, P.W., Patterson,
787 B.D., Thong, V.D., Ruedi, M., Hiller, M., et al. (2024). Distinct genes with similar functions
788 underlie convergent evolution in Myotis bat ecomorphs. Mol. Biol. Evol. *41*.
789 https://doi.org/10.1093/molbev/msae165.

790 106. Hanahan, D., and Weinberg, R.A. (2011). Hallmarks of Cancer: The Next Generation. Cell *144*,
791 646–674. https://doi.org/10.1016/j.cell.2011.02.013.

792 107. Hanahan, D., and Weinberg, R.A. (2000). The Hallmarks of Cancer. Cell *100*, 57–70.
793 https://doi.org/10.1016/S0092-8674(00)81683-9.

794 108. Hanahan, D. (2022). Hallmarks of Cancer: New Dimensions. Cancer Discov. *12*, 31–46.
795 https://doi.org/10.1158/2159-8290.CD-21-1059.

796 109. Milacic, M., Beavers, D., Conley, P., Gong, C., Gillespie, M., Griss, J., Haw, R., Jassal, B.,
797 Matthews, L., May, B., et al. (2024). The reactome pathway knowledgebase 2024. Nucleic
798 Acids Res. *52*, D672–D678. https://doi.org/10.1093/nar/gkad1025.

799 110. Ohtsuki, K., and Ono, Y. (1997). The biochemical mechanisms involved in the biological effects
800 induced by neocarzinostatin (NCS) and the NCS chromophore. In Neocarzinostatin (Springer
801 Japan), pp. 129–154. https://doi.org/10.1007/978-4-431-66914-2_7.

802 111. Bañuelos, A., Reyes, E., Ocadiz, R., Alvarez, E., Moreno, M., Monroy, A., and Gariglio, P.
803 (2003). Neocarzinostatin induces an effective p53-dependent response in human
804 papillomavirus-positive cervical cancer cells. J. Pharmacol. Exp. Ther. *306*, 671–680.
805 https://doi.org/10.1124/jpet.103.051557.

806 112. Ishida, N., Miyazaki, K., Kumagai, K., and Rikimaru, M. (1965). Neocarzinostatin, an Antitumor
807 Antibiotic of High Molecular Weight Isolation, Physicochemical Properties and Biological
808 Activities. The Journal of Antibiotics, Series A *18*, 68–76.
809 https://doi.org/10.11554/antibioticsa.18.2_68.

810 113. Abegglen, L.M., Caulin, A.F., Chan, A., Lee, K., Robinson, R., Campbell, M.S., Kiso, W.K.,

811 Schmitt, D.L., Waddell, P.J., Bhaskara, S., et al. (2015). Potential Mechanisms for Cancer
812 Resistance in Elephants and Comparative Cellular Response to DNA Damage in Humans.
813 JAMA *314*, 1850–1860. https://doi.org/10.1001/jama.2015.13134.

814 114. Firsanov, D., Zacher, M., Tian, X., Zhao, Y., George, J.C., Sformo, T.L., Tombline, G., Biashad,
815 S.A., Gilman, A., Hamilton, N., et al. (2023). DNA Repair and Anti-Cancer Mechanisms in the
816 Longest-Living Mammal: The Bowhead Whale. bioRxiv, 2023.05.07.539748.
817 https://doi.org/10.1101/2023.05.07.539748.

818 115. Lagunas-Rangel, F.A. (2020). Why do bats live so long?—Possible molecular mechanisms.
819 Biogerontology *21*, 1–11. https://doi.org/10.1007/s10522-019-09840-3.

820 116. Chionh, Y.T., Cui, J., Koh, J., Mendenhall, I.H., Ng, J.H.J., Low, D., Itahana, K., Irving, A.T.,
821 and Wang, L.-F. (2019). High basal heat-shock protein expression in bats confers resistance to
822 cellular heat/oxidative stress. Cell Stress Chaperones *24*, 835–849.
823 https://doi.org/10.1007/s12192-019-01013-y.

824 117. Hua, R., Ma, Y.-S., Yang, L., Hao, J.-J., Hua, Q.-Y., Shi, L.-Y., Yao, X.-Q., Zhi, H.-Y., and Liu,
825 Z. (2024). Experimental evidence for cancer resistance in a bat species. Nat. Commun. *15*,
826 1401. https://doi.org/10.1038/s41467-024-45767-1.

827 118. Peixoto, F.P., Braga, P.H.P., and Mendes, P. (2018). A synthesis of ecological and
828 evolutionary determinants of bat diversity across spatial scales. BMC Ecol. *18*, 18.
829 https://doi.org/10.1186/s12898-018-0174-z.

830 119. USGS (2022). North American Bat Ranges.
831 http://dds.cr.usgs.gov/pub/data/nationalatlas/bat000p010g_nt00373.tar.gz
832 http://dds.cr.usgs.gov/pub/data/nationalatlas/bat000p010g_nt00373.tar.gz.

833 120. Rhie, A., McCarthy, S.A., Fedrigo, O., Damas, J., Formenti, G., Koren, S., Uliano-Silva, M.,
834 Chow, W., Fungtammasan, A., Kim, J., et al. (2021). Towards complete and error-free genome
835 assemblies of all vertebrate species. Nature *592*, 737–746. https://doi.org/10.1038/s41586-
836 021-03451-0.

837 121. The Darwin Tree of Life Project Consortium (2022). Sequence Locally, Think Globally: The
838 Darwin Tree of Life Project. Proceedings of the National Academy of Sciences *119*,
839 e2115642118. https://doi.org/10.1073/pnas.2115642118.

840 122. Lewin, H.A., Richards, S., Lieberman Aiden, E., Allende, M.L., Archibald, J.M., Bálint, M.,
841 Barker, K.B., Baumgartner, B., Belov, K., Bertorelle, G., et al. (2022). The Earth BioGenome
842 Project 2020: Starting the Clock. Proceedings of the National Academy of Sciences *119*,
843 e2115635118. https://doi.org/10.1073/pnas.2115635118.

844 123. Slater, G.J., Goldbogen, J.A., and Pyenson, N.D. (2017). Independent evolution of baleen
845 whale gigantism linked to Plio-Pleistocene ocean dynamics. Proc. Biol. Sci. *284*.
846 https://doi.org/10.1098/rspb.2017.0546.

847 124. Tollis, M., Robbins, J., Webb, A., Kuderna, L.F.K., Caulin, A.F., Garcia, J.D., Bérubé, M.,
848 Pourmand, N., Marquès-Bonet, T., O'Connell, M., et al. (2019). Return to the sea, get huge,
849 beat cancer: An analysis of cetacean genomes including an assembly for the humpback whale
850 (Megaptera novaeangliae). Mol. Biol. Evol. *36*, 1746–1763.
851 https://doi.org/10.1093/molbev/msz099.

852 125. Nair, N.U., Cheng, K., Naddaf, L., Sharon, E., Pal, L.R., Rajagopal, P.S., Unterman, I., Aldape,

K., Hannenhalli, S., Day, C.-P., et al. (2022). Cross-species identification of cancer resistance-associated genes that may mediate human cancer risk. Sci. Adv. *8*, eabj7176. https://doi.org/10.1126/sciadv.abj7176.

126. Caulin, A.F., Graham, T.A., Wang, L.-S., and Maley, C.C. (2015). Solutions to Peto's paradox revealed by mathematical modelling and cross-species cancer gene analysis. Philos. Trans. R. Soc. Lond. B Biol. Sci. *370*, 20140222. https://doi.org/10.1098/rstb.2014.0222.

127. Vazquez, J.M., Pena, M.T., Muhammad, B., Kraft, M., Adams, L.B., and Lynch, V.J. (2022). Parallel evolution of reduced cancer risk and tumor suppressor duplications in Xenarthra. bioRxiv, e82558. https://doi.org/10.1101/2022.08.04.502824.

128. Beichman, A.C., Zhu, L., and Harris, K. (2024). The evolutionary interplay of somatic and germline mutation rates. Annu. Rev. Biomed. Data Sci. *7*, 83–105. https://doi.org/10.1146/annurev-biodatasci-102523-104225.

129. Cagan, A., Baez-Ortega, A., Brzozowska, N., Abascal, F., Coorens, T.H.H., Sanders, M.A., Lawson, A.R.J., Harvey, L.M.R., Bhosle, S., Jones, D., et al. (2022). Somatic mutation rates scale with lifespan across mammals. Nature *604*, 517–524. https://doi.org/10.1038/s41586-022-04618-z.

130. Bergeron, L.A., Besenbacher, S., Zheng, J., Li, P., Bertelsen, M.F., Quintard, B., Hoffman, J.I., Li, Z., St Leger, J., Shao, C., et al. (2023). Evolution of the germline mutation rate across vertebrates. Nature *615*, 285–291. https://doi.org/10.1038/s41586-023-05752-y.

131. Lollar, A. (2018). The Rehabilitation and Captive Care of Insectivorous Bats. Weatherford International: Houston, TX, USA.

132. Morales, A.E., Dong, Y., Brown, T., Baid, K., Kontopoulos, D.-G., Gonzalez, V., Huang, Z., Ahmed, A.-W., Bhuinya, A., Hilgers, L., et al. (2025). Bat genomes illuminate adaptations to viral tolerance and disease resistance. Nature *638*, 449–458. https://doi.org/10.1038/s41586-024-08471-0.

133. O'Shea, T.J., Cryan, P.M., Cunningham, A.A., Fooks, A.R., Hayman, D.T.S., Luis, A.D., Peel, A.J., Plowright, R.K., and Wood, J.L.N. (2014). Bat flight and zoonotic viruses. Emerg. Infect. Dis. *20*, 741–745. https://doi.org/10.3201/eid2005.130539.

134. Levesque, D.L., Boyles, J.G., Downs, C.J., and Breit, A.M. (2021). High Body Temperature is an Unlikely Cause of High Viral Tolerance in Bats. J. Wildl. Dis. *57*, 238–241. https://doi.org/10.7589/JWD-D-20-00079.

135. Kirkwood, T.B.L. (2017). The disposable soma theory. The evolution of senescence in the tree of life, 23–39.

136. Toshkova, N., Zhelyzkova, V., Reyes-Ruiz, A., Haerens, E., de Castro Deus, M., Lacombe, R.V., Lecerf, M., Gonzalez, G., Jouvenet, N., Planchais, C., et al. (2024). Temperature sensitivity of bat antibodies links metabolic state of bats with antigen-recognition diversity. Nat. Commun. *15*, 5878. https://doi.org/10.1038/s41467-024-50316-x.

137. Gutiérrez-Guerrero, Y.T., Ibarra-Laclette, E., Martínez Del Río, C., Barrera-Redondo, J., Rebollar, E.A., Ortega, J., León-Paniagua, L., Urrutia, A., Aguirre-Planter, E., and Eguiarte, L.E. (2020). Genomic consequences of dietary diversification and parallel evolution due to nectarivory in leaf-nosed bats. Gigascience *9*. https://doi.org/10.1093/gigascience/giaa059.

138. Camacho, J., Bernal-Rivera, A., Peña, V., Morales-Sosa, P., Robb, S., Russell, J., Yi, K., Wang, Y., Tsuchiya, D., Murillo-García, O.E., et al. (2023). Sugar assimilation underlying dietary evolution of Neotropical bats. bioRxiv, 2023.07.02.547432. https://doi.org/10.1101/2023.07.02.547432.

139. Mandl, J.N., Schneider, C., Schneider, D.S., and Baker, M.L. (2018). Going to bat(s) for studies of disease tolerance. Front. Immunol. *9*, 2112. https://doi.org/10.3389/fimmu.2018.02112.

140. Ray, D.A., Feschotte, C., Pagan, H.J.T., Smith, J.D., Pritham, E.J., Arensburger, P., Atkinson, P.W., and Craig, N.L. (2008). Multiple Waves of Recent DNA Transposon Activity in the Bat, Myotis Lucifugus. Genome Res. *18*, 717–728. https://doi.org/10.1101/gr.071886.107.

141. Thomas, J., Phillips, C.D., Baker, R.J., and Pritham, E.J. (2014). Rolling-circle transposons catalyze genomic innovation in a mammalian lineage. Genome Biol. Evol. *6*, 2595–2610. https://doi.org/10.1093/gbe/evu204.

142. Yashin, A.I., Wu, D., Arbeev, K., Yashkin, A.P., Akushevich, I., Bagley, O., Duan, M., and Ukraintseva, S. (2021). Roles of interacting stress-related genes in lifespan regulation: insights for translating experimental findings to humans. J. Transl. Genet. Genom. *5*, 357–379. https://doi.org/10.20517/jtgg.2021.26.

143. Wu, L., Zhu, X., Liu, Y., Zhao, D., Yu, B.C., Wei, Z., Lin, X., and Qi, L.S. (2025). Identification of replicative aging and inflammatory aging signatures via whole-genome CRISPRi screens. Genome Biol. *26*, 233. https://doi.org/10.1186/s13059-025-03683-7.

144. Bullido, M.J., Martínez-García, A., Tenorio, R., Sastre, I., Muñoz, D.G., Frank, A., and Valdivieso, F. (2008). Double stranded RNA activated EIF2 alpha kinase (EIF2AK2; PKR) is associated with Alzheimer's disease. Neurobiol. Aging *29*, 1160–1166. https://doi.org/10.1016/j.neurobiolaging.2007.02.023.

145. Vermillion, K.L., Anderson, K.J., Hampton, M., and Andrews, M.T. (2015). Gene expression changes controlling distinct adaptations in the heart and skeletal muscle of a hibernating mammal. Physiol. Genomics *47*, 58–74. https://doi.org/10.1152/physiolgenomics.00108.2014.

146. Lam, B., Kajderowicz, K.M., Keys, H.R., Roessler, J.M., Frenkel, E.M., Kirkland, A., Bisht, P., El-Brolosy, M.A., Jaenisch, R., Bell, G.W., et al. (2024). Multi-species genome-wide CRISPR screens identify GPX4 as a conserved suppressor of cold-induced cell death. bioRxivorg, 2024.07.25.605098. https://doi.org/10.1101/2024.07.25.605098.

147. Sone, M., and Yamaguchi, Y. (2024). Cold resistance of mammalian hibernators ~ a matter of ferroptosis? Front. Physiol. *15*, 1377986. https://doi.org/10.3389/fphys.2024.1377986.

148. Kaelber, J.T., Demogines, A., Harbison, C.E., Allison, A.B., Goodman, L.B., Ortega, A.N., Sawyer, S.L., and Parrish, C.R. (2012). Evolutionary reconstructions of the transferrin receptor of Caniforms supports canine parvovirus being a re-emerged and not a novel pathogen in dogs. PLoS Pathog. *8*, e1002666. https://doi.org/10.1371/journal.ppat.1002666.

149. Demogines, A., Abraham, J., Choe, H., Farzan, M., and Sawyer, S.L. (2013). Dual host-virus arms races shape an essential housekeeping protein. PLoS Biol. *11*, e1001571. https://doi.org/10.1371/journal.pbio.1001571.

150. Kerr, S.A., Jackson, E.L., Lungu, O.I., Meyer, A.G., Demogines, A., Ellington, A.D., Georgiou, G., Wilke, C.O., and Sawyer, S.L. (2015). Computational and functional analysis of the virus-receptor interface reveals host range trade-offs in New World arenaviruses. J. Virol. *89*,

936 11643–11653. https://doi.org/10.1128/JVI.01408-15.

937 151. Kaur, H., Kalayjian, R., Wu, K., Tassiopoulos, K., Palella, F., Taiwo, B., Bush, W., Hileman, C.,
938 Bedimo, R., Koletar, S., et al. (2022). Associations of L-Ferritin and Tim-1 with frailty measures
939 in people with HIV: a cross-sectional and longitudinal study. Lancet Healthy Longev. *3*, S5.
940 https://doi.org/10.1016/s2666-7568(22)00066-6.

941 152. Kim, J., Jo, Y., Cho, D., and Ryu, D. (2022). L-threonine promotes healthspan by expediting
942 ferritin-dependent ferroptosis inhibition in C. elegans. Nat. Commun. *13*, 6554.
943 https://doi.org/10.1038/s41467-022-34265-x.

944 153. Daghlas, I., and Gill, D. (2021). Genetically predicted iron status and life expectancy. Clin. Nutr.
945 *40*, 2456–2459. https://doi.org/10.1016/j.clnu.2020.06.025.

946 154. Perez, K., Ciotlos, S., McGirr, J., Limbad, C., Doi, R., Nederveen, J.P., Nilsson, M.I., Winer,
947 D.A., Evans, W., Tarnopolsky, M., et al. (2022). Single nuclei profiling identifies cell specific
948 markers of skeletal muscle aging, frailty, and senescence. Aging (Albany NY) *14*, 9393–9422.
949 https://doi.org/10.18632/aging.204435.

950 155. Trifunovic, A., Wredenberg, A., Falkenberg, M., Spelbrink, J.N., Rovio, A.T., Bruder, C.E.,
951 Bohlooly-Y, M., Gidlöf, S., Oldfors, A., Wibom, R., et al. (2004). Premature ageing in mice
952 expressing defective mitochondrial DNA polymerase. Nature *429*, 417–423.
953 https://doi.org/10.1038/nature02517.

954 156. Van Goethem, G., Dermaut, B., Löfgren, A., Martin, J.J., and Van Broeckhoven, C. (2001).
955 Mutation of POLG is associated with progressive external ophthalmoplegia characterized by
956 mtDNA deletions. Nat. Genet. *28*, 211–212. https://doi.org/10.1038/90034.

957 157. Cao, L., Li, W., Kim, S., Brodie, S.G., and Deng, C.-X. (2003). Senescence, aging, and
958 malignant transformation mediated by p53 in mice lacking the Brca1 full-length isoform. Genes
959 Dev. *17*, 201–213. https://doi.org/10.1101/gad.1050003.

960 158. Vijg, J., Perls, T., Franceschi, C., and van Orsouw, N.J. (2001). BRCA1 gene sequence
961 variation in centenarians. Ann. N. Y. Acad. Sci. *928*, 85–96. https://doi.org/10.1111/j.1749-
962 6632.2001.tb05639.x.

963 159. Fearon, E.R. (1997). Human cancer syndromes: clues to the origin and nature of cancer.
964 Science *278*, 1043–1050. https://doi.org/10.1126/science.278.5340.1043.

965 160. Donoho, G., Brenneman, M.A., Cui, T.X., Donoviel, D., Vogel, H., Goodwin, E.H., Chen, D.J.,
966 and Hasty, P. (2003). Deletion of Brca2 exon 27 causes hypersensitivity to DNA crosslinks,
967 chromosomal instability, and reduced life span in mice. Genes Chromosomes Cancer *36*, 317–
968 331. https://doi.org/10.1002/gcc.10148.

969 161. Wooster, R., Bignell, G., Lancaster, J., Swift, S., Seal, S., Mangion, J., Collins, N., Gregory, S.,
970 Gumbs, C., and Micklem, G. (1995). Identification of the breast cancer susceptibility gene
971 BRCA2. Nature *378*, 789–792. https://doi.org/10.1038/378789a0.

972 162. Sotgia, S., Zinellu, A., Mangoni, A.A., Serra, R., Pintus, G., Caruso, C., Deiana, L., and Carru,
973 C. (2017). Cellular immune activation in Sardinian middle-aged, older adults and centenarians.
974 Exp. Gerontol. *99*, 133–137. https://doi.org/10.1016/j.exger.2017.10.005.

975 163. Lee, K.-A., Flores, R.R., Jang, I.H., Saathoff, A., and Robbins, P.D. (2022). Immune
976 senescence, immunosenescence and aging. Front. Aging *3*, 900028.

977 https://doi.org/10.3389/fragi.2022.900028.

978 164. Yousefzadeh, M.J., Flores, R.R., Zhu, Y., Schmiechen, Z.C., Brooks, R.W., Trussoni, C.E., Cui,
979 Y., Angelini, L., Lee, K.-A., McGowan, S.J., et al. (2021). An aged immune system drives
980 senescence and ageing of solid organs. Nature *594*, 100–105. https://doi.org/10.1038/s41586-
981 021-03547-7.

982 165. Lee, C.-S., Chang, C.-H., Chen, C.-Y., Shih, C.-Y., Peng, J.-K., Huang, H.-L., Chen, P.-Y.,
983 Huang, T.-L., Chen, C.-Y., and Tsai, J.-S. (2022). Upregulation of cluster of differentiation 36
984 mRNA expression in peripheral blood mononuclear cells correlates with frailty severity in older
985 adults. J. Cachexia Sarcopenia Muscle *13*, 1948–1955. https://doi.org/10.1002/jcsm.13003.

986 166. Kimmel, J.C., Yi, N., Roy, M., Hendrickson, D.G., and Kelley, D.R. (2021). Differentiation
987 reveals latent features of aging and an energy barrier in murine myogenesis. Cell Rep. *35*,
988 109046. https://doi.org/10.1016/j.celrep.2021.109046.

989 167. Tian, Y., Lu, J., Hao, X., Li, H., Zhang, G., Liu, X., Li, X., Zhao, C., Kuang, W., Chen, D., et al.
990 (2020). FTH1 inhibits ferroptosis through ferritinophagy in the 6-OHDA model of Parkinson's
991 disease. Neurotherapeutics *17*, 1796–1812. https://doi.org/10.1007/s13311-020-00929-z.

992 168. Ricklefs, R.E. (2010). Life-history connections to rates of aging in terrestrial vertebrates. Proc.
993 Natl. Acad. Sci. U. S. A. *107*, 10314–10319. https://doi.org/10.1073/pnas.1005862107.

994 169. Tian, S., Zeng, J., Jiao, H., Zhang, D., Zhang, L., Lei, C.-Q., Rossiter, S.J., and Zhao, H.
995 (2023). Comparative analyses of bat genomes identify distinct evolution of immunity in Old
996 World fruit bats. Sci Adv *9*, eadd0141. https://doi.org/10.1126/sciadv.add0141.

997 170. Jonathan Sleeman, Center Director, USGS National Wildlife Health Center (2020). NWHC
998 Operations During the COVID-19 Pandemic and Information About Coronaviruses in Wildlife.

999 171. White-Nose Syndrome Disease Management Working Group National White-Nose Syndrome
1000 Decontamination Protocol.

1001 172. Wu, N., Nguyen, X.-N., Wang, L., Appourchaux, R., Zhang, C., Panthu, B., Gruffat, H., Journo,
1002 C., Alais, S., Qin, J., et al. (2019). The interferon stimulated gene 20 protein (ISG20) is an
1003 innate defense antiviral factor that discriminates self versus non-self translation. PLoS Pathog.
1004 *15*. https://doi.org/10.1371/journal.ppat.1008093.

1005 173. Legrand, A., Dahoui, C., De La Myre Mory, C., Noy, K., Guiguettaz, L., Versapuech, M., Loyer,
1006 C., Pillon, M., Wcislo, M., Guéguen, L., et al. (2024). SAMD9L acts as an antiviral factor
1007 against HIV-1 and primate lentiviruses by restricting viral and cellular translation. PLoS Biol. *22*,
1008 e3002696. https://doi.org/10.1371/journal.pbio.3002696.

1009 174. Išerić, H., Alkan, C., Hach, F., and Numanagić, I. (2022). Fast characterization of segmental
1010 duplication structure in multiple genome assemblies. Algorithms Mol. Biol.

1011 175. Brown, M., González De la Rosa, P.M., and Mark, B. (2023). A Telomere Identification Toolkit
1012 https://doi.org/10.5281/zenodo.10091385.

1013 176. Li, H. (2021). New strategies to improve minimap2 alignment accuracy. Bioinformatics.

1014 177. Goel, M., and Schneeberger, K. (2022). plotsr: visualizing structural similarities and
1015 rearrangements between multiple genomes. Bioinformatics *38*, 2922–2926.
1016 https://doi.org/10.1093/bioinformatics/btac196.

178. Minh, B.Q., Schmidt, H.A., Chernomor, O., Schrempf, D., Woodhams, M.D., von Haeseler, A., and Lanfear, R. (2020). IQ-TREE 2: New Models and Efficient Methods for Phylogenetic Inference in the Genomic Era. Mol. Biol. Evol. *37*, 1530–1534. https://doi.org/10.1093/molbev/msaa015.

179. Zhang, C., and Mirarab, S. (2022). Weighting by gene tree uncertainty improves accuracy of quartet-based species trees. Mol. Biol. Evol. *39*. https://doi.org/10.1093/molbev/msac215.

180. Romiguier, J., Ranwez, V., Delsuc, F., Galtier, N., and Douzery, E.J.P. (2013). Less is more in mammalian phylogenomics: AT-rich genes minimize tree conflicts and unravel the root of placental mammals. Mol. Biol. Evol. *30*, 2134–2144. https://doi.org/10.1093/molbev/mst116.

181. Dos Reis, M., and Yang, Z. (2019). Bayesian Molecular Clock Dating Using Genome-Scale Datasets. Methods Mol. Biol. *1910*, 309–330. https://doi.org/10.1007/978-1-4939-9074-0_10.

182. Yang, Z. (2007). PAML 4: phylogenetic analysis by maximum likelihood. Mol. Biol. Evol. *24*, 1586–1591. https://doi.org/10.1093/molbev/msm088.

183. Phillips, M.J. (2016). Geomolecular dating and the origin of placental mammals. Syst. Biol. *65*, 546–557. https://doi.org/10.1093/sysbio/syv115.

184. Gunnell, G.F., and Simmons, N.B. (2005). Fossil evidence and the origin of bats. J. Mamm. Evol. *12*, 209–246. https://doi.org/10.1007/s10914-005-6945-2.

185. Eiting, T.P., and Gunnell, G.F. (2009). Global Completeness of the Bat Fossil Record. J. Mamm. Evol. *16*, 151–173. https://doi.org/10.1007/s10914-009-9118-x.

186. Storch, G., Sigé, B., and Habersetzer, J. (2002). Tachypteron franzeni n. gen., n. sp., earliest emballonurid bat from the Middle Eocene of Messel (Mammalia, Chiroptera). Palaontol. Z. *76*, 189–199. https://doi.org/10.1007/bf02989856.

187. Ravel, A., Marivaux, L., Tabuce, R., Ben Haj Ali, M., Essid, E.L.M., and Vianey-Liaud, M. (2012). A new large philisid (Mammalia, Chiroptera, Vespertilionoidea) from the late Early Eocene of Chambi, Tunisia: LARGE BAT FROM CHAMBI. Palaeontology *55*, 1035–1041. https://doi.org/10.1111/j.1475-4983.2012.01160.x.

188. Lim, B.K. (2009). Review of the origins and biogeography of bats in South America. Chiroptera Neotropical *15*, 391–410.

189. Morgan, G.S., and Czaplewski, N.J. (2003). A New Bat (Chiroptera: Natalidae) from the Early Miocene of Florida, with Comments on Natalid Phylogeny. J Mammal *84*, 729–752. https://doi.org/10.1644/1545-1542(2003)084<0729:ANBCNF>2.0.CO;2.

190. Elliot, M.G., and Mooers, A.Ø. (2014). Inferring ancestral states without assuming neutrality or gradualism using a stable model of continuous character evolution. BMC Evol. Biol. *14*, 226. https://doi.org/10.1186/s12862-014-0226-8.

191. Kosakovsky Pond, S.L., Poon, A.F.Y., Velazquez, R., Weaver, S., Hepler, N.L., Murrell, B., Shank, S.D., Magalis, B.R., Bouvier, D., Nekrutenko, A., et al. (2020). HyPhy 2.5-A customizable platform for evolutionary hypothesis testing using PHYlogenies. Mol. Biol. Evol. *37*, 295–299. https://doi.org/10.1093/molbev/msz197.

192. Mendes, F.K., Vanderpool, D., Fulton, B., and Hahn, M.W. (2021). CAFE 5 models variation in evolutionary rates among gene families. Bioinformatics *36*, 5516–5518.

https://doi.org/10.1093/bioinformatics/btaa1022.

Materials and Methods

Data availability

All sequencing data and genomes generated in this study are available on NCBI under Bioprojects PRJNA973719, PRJNA1035541, and PRJNA1295526. Annotations generated in this study are available at https://github.com/docmanny/myotis-gene-annotations. All other code is available at https://github.com/sudmantlab/MyotisGenomeAssembly. All other data are archived on DataDryad at DOI: 10.5061/dryad.02v6wwqfh.

Samples and materials

All bats sampled for this study were wild caught under scientific collection permits for California and Arizona (see **Extended Data Table 1**). Bats were sampled using standard mist-netting procedures, including taking standard body measurements, following USGS recommendations for White-Nose Syndrome and COVID-19 prevention[170,171]. For *M. lucifugus*, the donor individual was field-caught in California and transported to the Genetics Laboratory of the California Department of Fish and Wildlife, where they were euthanized via isofluorane. The *M. velifer* individual was caught in Arizona and euthanized in the field via isoflurane. For both *M. lucifugus* and *M. velifer*, tissues were collected and preserved via flash-freezing in liquid nitrogen. All other genomes were generated from primary cell lines. Additional information can be found in the *Extended Methods* and in **Extended Data Table 1**.

All PKR experiments were performed using HeLa PKR-KO cells (kindly provided by A. Geballe, Fred Hutchinson Cancer Center, Seattle WA). The cells were maintained at 37°C with 5% CO_2 and cultured in DMEM supplemented with 5% fetal bovine serum (FBS), 1% penicillin/ streptomycin mix and 1 µg/mL puromycin (Sigma-Aldrich). All transfections were performed 24 hours after seeding, using 3 µL of TransIT-LT1 Transfection Reagent (Mirus Bio) per 1 µg of DNA and Opti-MEM media. We used previously-generated pSG5-FLAGx2 vectors encoding either *M. myotis* PKR1 (GenBank OP006550), *M. myotis* PKR2 (GenBank OP006559), *M. velifer* PKR1 (GenBank OP006558), or *M. velifer* PKR2 (GenBank OP006557)[30]. Plasmids encoding the interferon-stimulated gene ISG20[172] and a constitutively active variant of the sterile alpha motif domain-containing protein 9-like SAMD9L-F886Lfs*11 (here, SAMD9L[173]) were used as controls in viral infections and cell translation experiments, respectively.

Near-complete genome assembly and annotation

Details on DNA extraction, preparation of PacBio HiFi and Omni-C (Dovetail Genomics) libraries, and genome assembly and manual curation can be found in the *Extended Methods*.

Gene & repetitive element annotation and alignments

1089 Details describing our procedure for identifying and annotation repetitive elements and protein-
1090 coding gene annotations can be found in the *Extended Methods.*

1091 RNA sequencing for gene annotations and differential expression

1092 Details on RNA extraction, library preparation, sequencing, and can be found in the *Extended Methods* and
1093 **Extended Data Table 9**.

1094 Structural variation

1095 To understand the distribution of structural variants, including segmental duplication events, we used
1096 SyRI (Synteny and Rearrangement Identifier[65]) and BISER (Brisk Inference of Segmental duplication
1097 Evolutionary stRucture[174]). We first masked telomere regions using TIDK (Telomere Identification toolKit[175]),
1098 and mapped the primary 22 scaffolds of the nearctic *Myotis* genomes to each other with minimap2[176]. The
1099 scaffold corresponding to the X chromosome was omitted because there is no corresponding scaffold in the
1100 *M. yumanensis* assembly. To verify homologous chromosomes and fix strand orientation, we used *fixchr*
1101 from the SyRI package and manually renamed scaffolds accordingly, then re-mapped them with minimap2.
1102 We ran SyRI on the resulting files and plotted the results with plotsr[177]. We ran BISER on the primary 22
1103 scaffolds of the nearctic *Myotis* genomes with –keep-contigs and default settings to generate bed files with
1104 the inferred segmental duplication regions.

1105 Gene Trees & Phylogeny

1106 A phylogeny of all 536 mammals in our alignments was generated using IQTREE[178] (version 2.3.1)
1107 using all gene alignments with the settings "-B 1000 -m GTR+F3x4+R6." To generate gene trees, we first
1108 filtered our gene alignments to exclude alignments with over 50% gaps in the sequence and less than 4
1109 species. With the remaining alignments, we used IQTREE to find the best-fitting substitution model and tree
1110 using settings "--wbtl --bnni --alrt 1000 -B 1000 --safe". The best substitution models for each gene were
1111 saved as a NEXUS file. As the bootstrap values for this tree were unanimously 100%, we further confirmed
1112 the species tree by using ASTRAL-IV[179] (v1.24.4.7) using the settings "-t 54 -u 2 -C", and confirmed that our
1113 phylogeny agreed with other previously-published *Eutherian* phylogenies, including phylogenies of 39
1114 mammals[180], of 241 placental mammals[58], and of 11 nearctic *Myotis* species[56].

1115 Time-calibration of 59 bat genomes

1116 Using our codon alignments of 59 bat genomes, we generated a time-calibrated phylogeny using
1117 mcmctree[181] and PAML[182] (v. 4.10.0) using an approximate likelihood method. Using the pan-bat codon
1118 alignments and our phylogeny as input, with fossil calibrations based on previously published work[9,44,58,183–
1119 189], we ran *mcmctree* twice to generate the Hessian matrix and confirm convergence. This was followed by
1120 10 independent chains using the "out.BV" file from the first run. Finally, the output files of all 10 chains were
1121 combined to compute final divergence time estimates (see Extended Data Table 2).

1122 # Ancestral Body Size, Lifespan, and Cancer Risk reconstruction

1123 To explore how body size and lifespan have evolved over time in mammals, we used a super-
1124 phylogeny of mammal species[55] subsampled to only contain species with extant body size and lifespan data
1125 collected from AnAge[18] and PanTHERIA[19]. Ancestral body sizes and lifespans were simulated separately
1126 using StableTraits[190] and the settings "*--iterations 100000 --skip 1000 --chains 8*". Estimates were further
1127 validated by comparing our initial results to a second run of StableTraits using the same settings. To test the
1128 robustness of RICR against phylogenetic uncertainty, we repeated these simulations using 5,182/10,000 of
1129 the alternative topologies for the mammalian tree published in Upham *et al*. (2019).

1130 # Selection Scans & Evolutionary Rates

1131 ## aBSREL

1132 To conservatively test for branch-specific selection, we used aBSREL[100,191] (version 2.5.48) to test
1133 for selection at each branch within the nearctic *Myotis* clade for 15,734 gene alignments spanning 536
1134 mammals. These genes were identified as 1:1 orthologs across the full alignment, with no more than 50%
1135 sequence gaps and at least 4 species present in the alignment. For each gene alignment, the full phylogeny
1136 was trimmed to match the species present, and the HYPHY script "label-tree.bf" was used to highlight all
1137 nodes within nearctic *Myotis* as foreground branches. aBSREL was then run using the pruned and
1138 highlighted tree and gene alignments on the command line with the options "--code Universal --branches
1139 Foreground". We defined a gene as under selection if one or more regions within the gene demonstrated a
1140 selective pressure with an FDR-corrected p-value ≤ 0.05; a gene was specifically identified as under positive
1141 selection if at least one of these significant regions had an $\omega>1$.

1142 ## BUSTED

1143 To quantify the total amount of positive selection across the *Myotis* tree or the different species trees
1144 used in this manuscript, we used an improved version of the BUSTED[72,191] test called BUSTED-MH (see
1145 *Extended Methods* for details on BUSTED vs BUSTED-MH). We applied BUSTED-MH to 19,646 *Myotis*
1146 orthologous CDS alignments with at least five orthologs. These orthologs are cases where the Orthofinder
1147 gene trees coincide with the species tree. This effectively removes issues regarding whether we should use
1148 the gene or the species tree, at the cost of removing 2,110 genes from the *Myotis* selection analysis. Similarly,
1149 we applied BUSTED-MH to 17,469 non-*Myotis* bat alignments with at least five orthologs. The species in
1150 these two sets (*Myotis* bats and non-*Myotis* bats) are mutually exclusive. This includes a subset of 14,091
1151 alignments with orthologs present in two thirds of the non-*Myotis* bat species, regardless of the genes'
1152 presence/absence in the *Myotis*-only complement. This is specifically used to show that patterns of virus-
1153 driven adaptation are representative of all bats. We also tested 17,890 primate alignments with at least five
1154 orthologs with BUSTED-MH, as well as 19,311 glire, 18,000 carnivora and 18,504 ungulate alignments.

1155 ## Enrichment scores for VIPs

1156 We expanded on the set of VIPs reported in Souilmi *et al*. (2021)[73] (5,291 VIPs) by searching the
1157 literature for more recent publications reporting VIPs, with a final dataset of 5,527 VIPs. These VIPs ("All

1158 VIPs") were further sub-categorized into 4 groups based on their interactions with either DNA viruses and/or
1159 RNA viruses: "DNA VIPs", "DNA-only VIPs", "RNA VIPs", and "RNA-only VIPs" (**Extended Data Table 5**).
1160 For each VIP set, we selected sets of matching control genes by controlling for 16 different criteria. (Extended
1161 Data Table 5). Sets of control genes were resampled in a bootstrap procedure to generate 95% confidence
1162 intervals for sets of genes across a range of p-values; additional details can be found in the *Extended*
1163 *Methods*.

1164 Gene Duplications and CAFE analysis

1165 To quantify patterns of gene duplication and loss, we quantified the copy number of genes with human
1166 orthologs from our gene annotations for each nearctic *Myotis* genome. To calculate per-gene expansion and
1167 loss rates and their statistical significance, we ran CAFE[192] v5 on the previously described set of copy number
1168 counts using our time-calibrated species tree pruned to include only the nine nearctic *Myotis* species. CAFE
1169 uses a birth-death model of gene family evolution to investigate changes in gene family size accounting for
1170 evolutionary history using the species phylogeny. Evolutionary branch length is incorporated into the model
1171 expectations, thus accounting for potential bias resulting from differences in branch lengths. We ran CAFE
1172 on the subset of genes with two or more copies in at least one species using a Poisson distribution for the
1173 root frequency (*-p*), first generating an error model to correct for genome assembly and annotation error (-
1174 *e*). We compared the base model (each gene family belongs to the same evolutionary rate category) to
1175 gamma models (each gene family can belong to one of *k* evolutionary rate categories) with different values
1176 of *k* from 2 to 13. A final gamma model with *k*=9 was chosen to balance model log likelihood with the number
1177 of gene families for which the optimizer failed. The model was run three separate times to ensure
1178 convergence.

1179 To understand if genes in these pathways have higher birth rates or are more likely to have significant
1180 changes in gene copy number than expected relative to other genes, we evaluated the gene copy birth rate
1181 λ and number of genes that have significantly expanded or contracted in copy number on at least one branch
1182 within our nearctic *Myotis* phylogeny using a bootstrap procedure. Following Huang et al.[42], we tested if VIP
1183 genes in particular underwent significant copy number changes or had significantly different birth/death rates
1184 than non-VIP genes. For each category of VIP genes (all VIPs, DNA VIPs, DNA only VIPs, RNA VIPs, and
1185 RNA only VIPs), we generated 100 bootstrap sets of control non-VIP genes with the same number of genes
1186 as the corresponding VIP gene set. We ran CAFE on each set of VIP genes and the corresponding control
1187 non-VIP genes to infer per-gene birth-death rates and per-gene, per-branch expansion/loss events.

1188 Assessment of DNA Double-Strand Break Tolerance

1189 We assessed each species' tolerance to DNA double strand breaks using a by measuring viability,
1190 cytotoxicty, and apoptosis across a range of doses of Neocarzinostatin, a radiomimetic drug. We measured
1191 dose response curves in wing-derived primary dermal fibroblasts across 5 bat species (*Myotis lucifugus*, n=8;
1192 *Myotis evotis*, n=8; *Rousettus langosus*, n=2; *Eidolon helvum*, n=2; *Pteropus rodrigensis*, n=2) using the
1193 multiplexed ApoTox-Glo assay (Promega). Using 96-well plates, two individuals and 11 doses were assessed
1194 simultaneously with four technical replicates. Results were normalized to treatment controls for each
1195 individual in R as previously described[36,37,40,45].

1196 # PKR1/2 Characterization in PKR-KO HeLa cells

1197 ## Western blot

1198 We assessed for the steady state protein expression of *M. myotis* Flag-PKRs after transfection of 350
1199 ng or 700 ng total of DNA plasmids encoding: PKR1 alone, PKR2 alone or both PKR1 and PKR2 (175 ng of
1200 each and 350 ng of each, respectively). Briefly, cells were re-suspended and lysed in ice-cold RIPA buffer
1201 (50 mM Tris pH8, 150 mM NaCl, 2 mM EDTA, 0.5% NP40) with protease inhibitor cocktail (Roche) and
1202 sonicated. 20 µL of the clarified fraction was denatured with 5 µL of 6x Laemmli buffer at 95°C for 5 min and
1203 loaded into 4-20% BioRad Criterion TGX Stain-Free precast gel. The wet transfer into a PVDF membrane
1204 was executed overnight at 4°C. The membranes were blocked in a 1xTBS-T buffer (Tris HCl 50 mM pH8,
1205 NaCl 30 mM, 0.05% of Tween 20) containing 10 % powder milk, and were incubated for 1h. The membranes
1206 were incubated with primary mouse anti-Flag (Sigma F3165) and anti-Tubulin (Sigma T5168) antibodies and
1207 secondary anti-Mouse IgG-Peroxidase conjugated (Sigma A9044). Detection was made using the Chemidoc
1208 Imaging System (BioRad) with SuperSignal West Pico Chemiluminescent Substrate (ThermoFisher
1209 Scientific).

1210 ## Luciferase reporter assays

1211 Luciferase reporter assays were carried out to investigate whether the two PKR paralogs have
1212 synergistic, additive or dominant negative effect in translation shutdown. 25,000 PKR-KO cells were seeded
1213 in 24-well plates. The next day, cells were transfected with 350 ng of empty pSG5, 350 ng of PKR1, 350 ng
1214 of PKR2, or 175 ng of PKR1+ 175 ng of PKR2, with additional 50 ng of FFLuc firefly luciferase reporter
1215 plasmid per well. Sterile alpha motif domain-containing proteins 9L (SAMD9L gain-of-function mutant) was
1216 used as a positive control of translational repression[173]. 24 h post transfection, cells were washed with PBS,
1217 lysed by a 5× reporter lysis buffer (Promega) and incubated overnight at -20°C. Cells were then collected
1218 and 100 µl of the luciferase substrate (Promega) was added to 20 µl of the lysis supernatant. Alternatively,
1219 cells were lysed using BrightGlow Lysis Reagent (Promega E2620). The relative luminescence units (RLUs)
1220 proportional to the translation of the luciferase reporter were immediately quantified with LUMIstar Omega
1221 microplate reader optima (BMG Labtech). All luciferase assays were conducted in technical duplicates in at
1222 least five independent experiments. Fold change results were normalized to the empty pSG5 condition within
1223 each independent experiment.

1224 ## PKR co-immunoprecipitation

1225 Hela PKR-KO cells were transfected with 1.25µg plenti6 HA-tagged *M. myotis* PKR1 plasmid per million cells
1226 and 1.25µg of either plenti6 myc empty vector, myc-tagged *M. myotis* PKR1 or myc-tagged *M. myotis* PKR2
1227 plasmid using TransIT-LTI transfection reagent (Mirus Bio). The next day, some wells were infected with
1228 Sindbis virus expressing GFP (SINV-GFP) at MOI 2 for 24 hours. Cells were then scraped with cold PBS
1229 and pelleted. For the IP, cells were lysed in 500µl IP buffer (50mM Tris HCl pH7.5, 140mM NaCl, 6 mM
1230 MgCl2, 0.1% NP40) supplemented with RNase (RiboLock, Fisher Scientific) and protease (complete EDTA-
1231 free protease inhibitor cocktail, Sigma) inhibitors for 10 minutes on ice, then centrifuged at 12,000 *xg* for 10
1232 min at 4°C. 5% of the volume was kept for input, while the rest was incubated with 40µl µMACS anti-c-myc
1233 MicroBeads (Miltenyi Biotec) for 1h at 4°C with constant rotation. Samples were then loaded onto µMACS
1234 columns placed in the magnetic field of a µMACS Separator (Miltenyi Biotec), washed 4 times with cold IP
1235 buffer, and eluted with the µMACS denaturing elution buffer. Proteins were denatured in elution buffer for 5

1236 min at 95°C, then loaded onto a 4-20% BioRad Criterion TGX Stain-Free precast gel and transferred onto
1237 an Amersham Protran nitrocellulose membrane (Sigma) for 1h. Membranes were blocked for 1h in 5% milk
1238 in PBS (Euromedex) supplemented with 0.2% tween (Fisher) and incubated with mouse anti-myc monoclonal
1239 antibodies (Abcam 9E10, cat# ab32) then secondary anti-mouse IgG antibodies conjugated with HRP
1240 (Sigma, cat# A4416), or with rat anti-HA antibodies conjugated with HRP (Roche, Sigma, cat#
1241 12013819001). Images were taken on a Fusion FX imager (Vilber) with SuperSignal West Femto
1242 Chemiluminescent Substrate (ThermoFisher Scientific).

1243 Cell viability assay

1244 Hela PKR-KO cells were transfected 24h after plating in 96 well plates (n=10,000 cells/well), with 100
1245 or 200 ng of pSG5 plasmid: empty or coding for *M. myotis* or *M. velifer* PKR1, PKR2 or PKR1+2 equal mix
1246 (50%-50%). 24 hours post-transfection, positive control cells were treated with an apoptosis-inducing drug,
1247 Etoposide, at different doses (250, 200 or 100 µM). 48 hours post transfection, cells were harvested and
1248 lysed to quantify luminescent signal according to CellTiter-Glo® Luminescent Cell Viability Assay (Promega)
1249 kit protocol.

1250 VSV and SINV infections

1251 VSV infections. 200,000 cells were plated in 12-well and transfected 24 h after with 350 ng of pSG5
1252 plasmid: empty, or encoding *M. myotis* or *M. velifer* PKR1, PKR2, or equal input of PKR1 and PKR2 (175 ng
1253 per plasmid), or a plasmid encoding interferon-stimulated exonuclease gene 20 (ISG20), due to its known
1254 antiviral activity against VSV as positive control[172]. Cells were infected 24 h post transfection with replicative
1255 VSV-GFP virus[70] at a MOI of 3. Cells were fixed with 4% paraformaldehyde 16-18 hours post infection. VSV
1256 infection was quantified by measuring the percentage of GFP positive cell populations with BD FACSCanto
1257 II Flow Cytometer (SFR BioSciences). Fold change results were normalized to the empty pSG5 condition
1258 across at least three independent experiments.

1259 SINV infections. Hela PKR-KO cells were transfected with 5µg pSG5 empty vector, *M. myotis* PKR1,
1260 *M. myotis* PKR2 or 2.5µg *M. myotis* PKR1 + 2.5µg *M. myotis* PKR2 per million cells using TransIT-LTI
1261 transfection reagent (Mirus Bio). The next day, some wells were infected with SINV-GFP at MOI 0.2. Cells
1262 were then placed into a CellCyte X live cell imaging system (Cytena) and pictures of every well were taken
1263 every 2h for 48h. The fraction of GFP+ cells over the total cell area was measured and averaged from six
1264 photos of 2 individual wells per condition, and repeated for a total of three independent experiments.

Fig. Legends

Fig. 1: 8 near-complete reference assemblies for North American (nearctic) *Myotis*. A) Phylogeny of 38 bat genomes with 3 outgroup species: cow *(bosTau9*), mouse (*mm39*); and human (*T2T-CHM13v2.0*). Bars at the tips of the phylogeny indicate the Area under the NGx curve (AuNG) score of each genome, a metric of genome contiguity independent of genome size. The dotted line represents the AuNG score for the T2T-CHM13v2.0 assembly. **B)** The time-calibrated phylogeny of 9 nearctic and two representative Palaearctic *Myotis* species based on orthologous codon alignments. Blue bars represent age uncertainties. The branch highlighted in red (*M. volans* as outgroup to the other nearctic *Myotis*) has 100% bootstrap support, but 0% local posterior probability support. **C)** Map of capture sites for new cell lines with representative images for the species sequenced in this study (see "Acknowledgements" for attributions). **D)** Mammalian BUSCO scores for annotations generated for the 8 new *Myotis* genomes. **E)** Ideogram bar plot indicating completion status of each chromosome in assembly. Pie graphs indicate completion status of all chromosomes in assembly. Percentages above ideogram indicate the proportion of T2T assembled chromosomes across species. All chromosomes were positively identified based on size, synteny, and homology to human chromosomes[51]. "Complete (T2T)" status indicates that a chromosome is fully assembled telomere-to-telomere without gaps; "Draft (T2T, gaps)" status indicates that a chromosome is fully scaffolded with both telomeres, but has one or more gaps in the assembly; "Incomplete" status indicates that a chromosome was positively identified, but was not scaffolded from telomere to telomere (only contains one telomere).

Fig. 2: A varied structural variation landscape across 9 nearctic *Myotis* species. A) Synteny between chromosomes of 9 *Myotis* species showing syntenic regions (grey), inversions (orange), translocations (green), and duplications (blue). **B)** Distribution of transposable elements (top) and segmental duplications (red heatmap, bottom) in *M. velifer*. Putative locations of centromeres are denoted by the dotted lines. **C)** Pie chart of overall genomic proportions of TEs in *M. velifer*. **D)** Histogram of segmental duplication size distributions genome-wide in *M. velifer*.

Fig. 3: Evolutionary history and function of an actively segregating copy number polymorphism of *PKR* in *Myotis*. A) Structural comparison of the main PKR haplotypes in two species. Orthologous regions between the two haplotypes are indicated by grey bands, while syntenic duplications are indicated in green. Exons are annotated with black marks. **B)** Cartoon of the PKR locus in the two phased haplotype assemblies of each species. While *PKR2* is present across all haplotypes, *PKR1* and *PKR copy 3* are polymorphic within and across species. Each number indicates the number of exons per gene. **C)** Reconciled gene tree for *PKRs* across all haplotypes and species shown in B. Haplotype corresponding to the reference (A) and alternate (B) haplotype for each species are represented by upper- and lower-diagonal triangles, respectively. **D)** Effect of Myotis PKR expression on luciferase reporter translation in PKR-KO cells, measured in Relative Light Units (RLU) and normalized to the empty pSG5 control. Human SAMD9L-GoF is a positive control of translation inhibition[173]. **E-F)** Effect of PKR on viral infection by VSV-GFP (E, and S3B) and SINV-GFP (F 34h post-infection, and S3C), measured by flow cytometry as the % of GFP+ cells, normalized to the pSG5 control. Although all conditions restricted VSV and SINV, the expression of both PKR1+PKR2 was not beneficial against these viral infections. ISG20 served as a positive control of VSV-GFP restriction[172]. **G)** Co-immunoprecipitation (IP) of PKR-KO cells transfected with *Myotis* HA-PKR1 and either *Myotis* myc-PKR1, *Myotis* myc-PKR2 or a myc-empty vector control. Proteins were pulled down with anti-myc beads and lysates from 5% input or IP samples were run on a western blot and stained for HA and myc. Representative of 3 independent experiments. Extended Data Fig. 3E for SINV conditions. H, Quantification of the three independent experiments (mock and SINV): HA left and myc right. For **D-F**, error bars indicate the means ± SEM for at least three independent experiments. Statistics, unpaired t-test ($p<0.05$). mPKR, Myotis myotis PKR; vPKR, Myotis velifer PKR. For gel source data, see Supplementary Figure 1.

1313 **Fig. 4: Adaptation to DNA viruses, but not RNA viruses, is enriched in *Myotis* and other bats. A)** Diagram
1314 of an example VIP, host cell transmembrane receptor CD45, showing strength of adaptation at each codon and
1315 the locations of direct interactions with the human adenovirus protein sec49K. **B-F)** Enrichment plots showing
1316 the ratio of positive selection in only *Myotis* bats in VIPs versus matched sets of control genes at different p-
1317 value thresholds. The solid line shows the median ratio; the color of the line, and the number above each point,
1318 represents the number of VIPs with significant BUSTED-MH p-values at the given threshold; the grey band
1319 represents the 95% confidence interval generated by bootstrapping sets of matched control genes. The number
1320 above each point indicates the number of VIP genes and sampled control genes used for each ratio calculation.
1321 The 95% confidence interval widens at lower p-values because there are fewer VIPs with significant p-values
1322 as the alpha threshold decreases, reducing power. **G-I)** The same as above, across all bats in this study
1323 excluding *Myotis*. **J-L)** The number of VIP genes inferred by CAFE to have significantly expanded or contracted
1324 in copy number on at least one branch of the nearctic *Myotis* phylogeny (blue line) compared to the distribution
1325 across 100 randomized sets of non-VIP control genes (black line). Vertical dashed lines indicated the 95%
1326 highest density interval for the control gene distribution.
1327
1328 **Fig. 5: Evolution of cancer risk and resistance in *Myotis* and other mammals. A, B)** Cophylo plot of the
1329 evolution of body size (**A**) and lifespan (**B**) across *Eutheria*. Branch lengths in **A-B** are scaled proportional to
1330 the rate of change of the trait over time. **C)** The phylogeny of nearctic *Myotis* species with inset pie charts
1331 representing the proportion of the top 100 Reactome pathways overrepresented among genes under selection
1332 at each node that are associated with cancer-related processes. Below, pie chart indicates expected proportion
1333 of pathways are cancer-associated after 1000 random samples of 100 pathways from the full Reactome
1334 database. Asterisks represent nodes with proportions greater than the expected value at $p \leq 0.05$ using Fisher's
1335 exact test. **D)** Proportion of the top 100 Reactome pathways overrepresented among genes under selection
1336 across all nodes in a species' evolutionary history that are associated with cancer-related processes. **E)** Volcano
1337 plot of overrepresented pathways in Reactome among the union set of genes under selection across all nodes
1338 in the evolutionary history for *M. lucifugus*. **F)** Viability and Apoptosis fold-change in 5 bat species in response
1339 to different doses of neocarzinostatin (NCS), a potent inducer of DNA double-strand breaks. Points represent
1340 individual replicates normalized to each species' control, while bars represent mean ± 95% confidence intervals.
1341
1342 **Fig. 6**: **Pleiotropy among genes under selection in *M. lucifugus* between DNA-damage responsive genes**
1343 **and DNA-only VIPs. A-B)** Volcano plots of genes that are differentially expressed in *M. lucifugus* after 6 hours
1344 (**A**) and 18 hours (**B**) of treatment with 100nM neocarzinostatin (NCS). **C-D)** Pathway-level Gene Set
1345 Enrichment Analysis (GSEA) of genes differentially expressed at 6 and 18 hours post-treatment. **E)** Upset plot
1346 between genes that are differentially expressed after NCS treatment and DNA-only VIPs; the hypergeometric
1347 P-value of the intersection is shown. **F)** Pathway-level overrepresentation analysis of genes that are DNA-only
1348 VIPs and are also differentially expressed in response to NCS treatment. **G)** Pathway-level overrepresentation
1349 analysis of genes identified as under selection in *M. lucifugus* via ABSREL that are DNA-only VIPs and are also
1350 differentially expressed in response to NCS treatment.
1351
1352

Extended Data

Extended Data Fig. 1-7:

1. **Contiguity statistics for 8 novel *Myotis* genomes**
2. **Estimated node divergence times for *Chiroptera* and ASTRAL-IV scores.**
3. **Correlations of TEs and structural variation in *Myotis* genomes**
4. **Additional functional characterization of *Myotis* PKR duplicates**
5. **VIP selection enrichments in bats and other mammals**
6. **Evolution of Body Size and Lifespan across *Myotis***
7. **Genes differentially expressed after neocarzinostatin treatment and their overlap with DNA-only VIPs**

Extended Data Table 1. Genome Statistics
Extended Data Table 2. Accessions for additional genomes used in this study
Extended Data Table 3. SyRI-identified structural variants (SVs)
Extended Data Table 4. Experimental data for PKR experiments
Extended Data Table 5. List of VIPs and VIP subclasses
Extended Data Table 6. Ancestral State Reconstructions for body size and lifespan in mammals
Extended Data Table 7. aBSREL significant gene lists and Reactome enrichments
Extended Data Table 8. Experimental data for Neocarzinostatin experiments
Extended Data Table 9. RNA-seq QC statistics and GSEA results

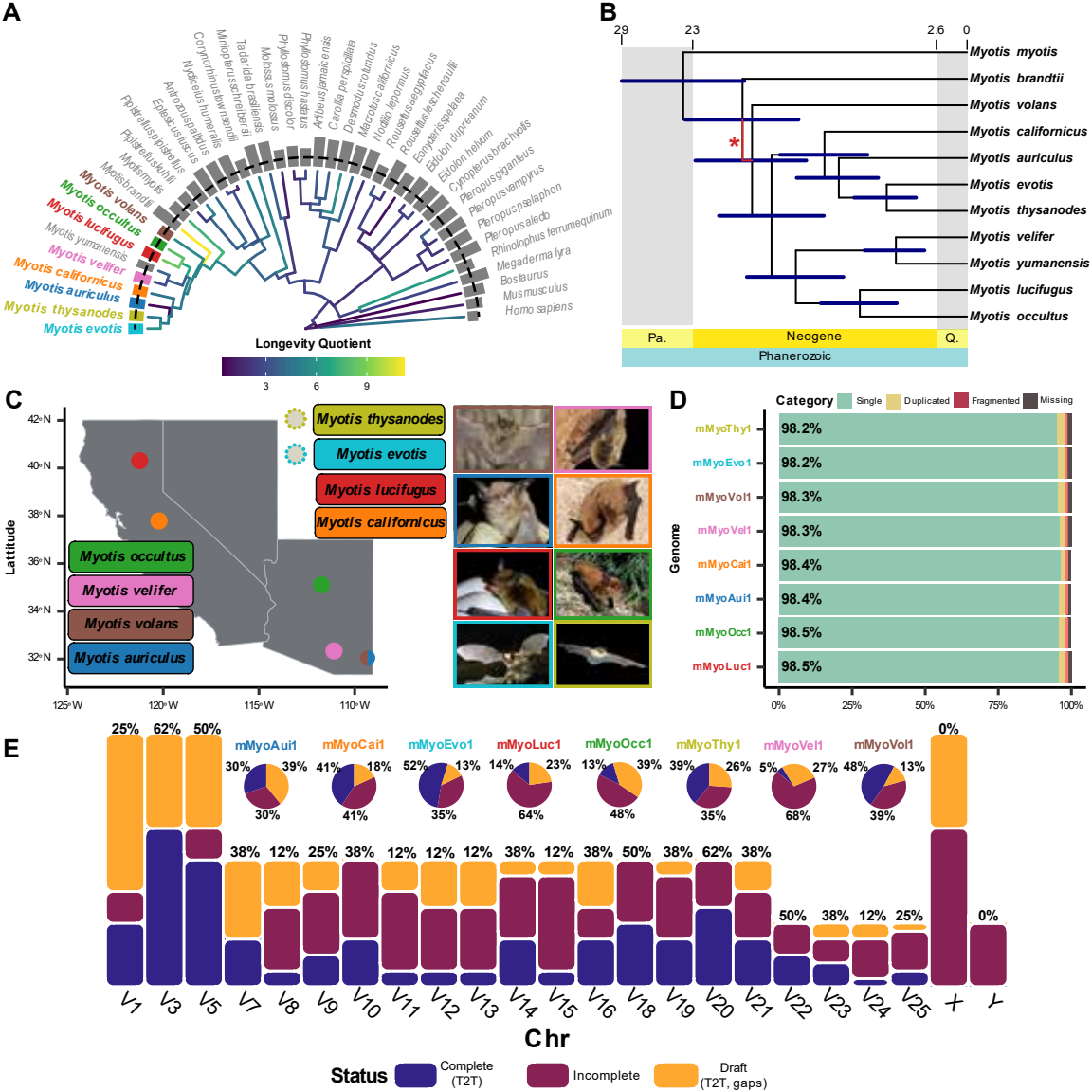
A
Corynorhinus townsendii
Miniopterus schreibersii
Nycticeius humeralis
Eptesicus fuscus
Antrozous pallidus
Pipistrellus pipistrellus
Pipistrellus nathusii
Myotis brandtii
Myotis myotis
Myotis volans
Myotis lucifugus
Myotis yumanensis
Myotis velifer
Myotis californicus
Myotis auriculus
Myotis thysanodes
Myotis evotis
Tadarida brasiliensis
Molossus molossus
Phyllostomus discolor
Phyllostomus hastatus
Artibeus jamaicensis
Carollia perspicillata
Desmodus rotundus
Macrotus californicus
Noctilio leporinus
Rousettus aegyptiacus
Rousettus leschenaultii
Eonycteris spelaea
Eidolon dupreanum
Eidolon helvum
Cynopterus brachyotis
Pteropus gigantheus
Pteropus vampyrus
Pteropus pselaphon
Pteropus aldebo
Pteropus ferrumequinum
Rhinolophus ferrumequinum
Megaderma lyra
Bos taurus
Mus musculus
Homo sapiens
Longevity Quotient
3
6
9
B
29
23
2.6
0
Myotis myotis
Myotis brandtii
Myotis volans
Myotis californicus
Myotis auriculus
Myotis evotis
Myotis thysanodes
Myotis velifer
Myotis yumanensis
Myotis lucifugus
Myotis occultus
*
Pa.
Neogene
Q.
Phanerozoic
C
Myotis thysanodes
Myotis evotis
Myotis lucifugus
Myotis californicus
Myotis occultus
Myotis velifer
Myotis volans
Myotis auriculus
Latitude
42° N
40° N
38° N
36° N
34° N
32° N
125° W
120° W
115° W
110° W
D
Category
Single
Duplicated
Fragmented
Missing
Genome
mMyoThy1 98.2%
mMyoEvo1 98.2%
mMyoVol1 98.3%
mMyoVel1 98.3%
mMyoCal1 98.4%
mMyoAui1 98.4%
mMyoOcc1 98.5%
mMyoLuc1 98.5%
0%
25%
50%
75%
100%
E
mMyoAui1
mMyoCal1
mMyoEvo1
mMyoLuc1
mMyoOcc1
mMyoThy1
mMyoVel1
mMyoVol1
25% 62% 50% 0%
30% 39% 30%
41% 18% 41%
52% 13% 35%
14% 23% 64%
13% 39% 48%
39% 26% 35%
5% 27% 68%
48% 13% 39%
38% 12% 25% 38% 12% 12% 12% 38% 12% 38% 50% 38% 62% 38%
50% 38% 12% 25%
0%
V1 V3 V5 V7 V8 V9 V10 V11 V12 V13 V14 V15 V16 V18 V19 V20 V21 V22 V23 V24 V25 X Y
Chr
Status
Complete (T2T)
Incomplete
Draft (T2T, gaps)

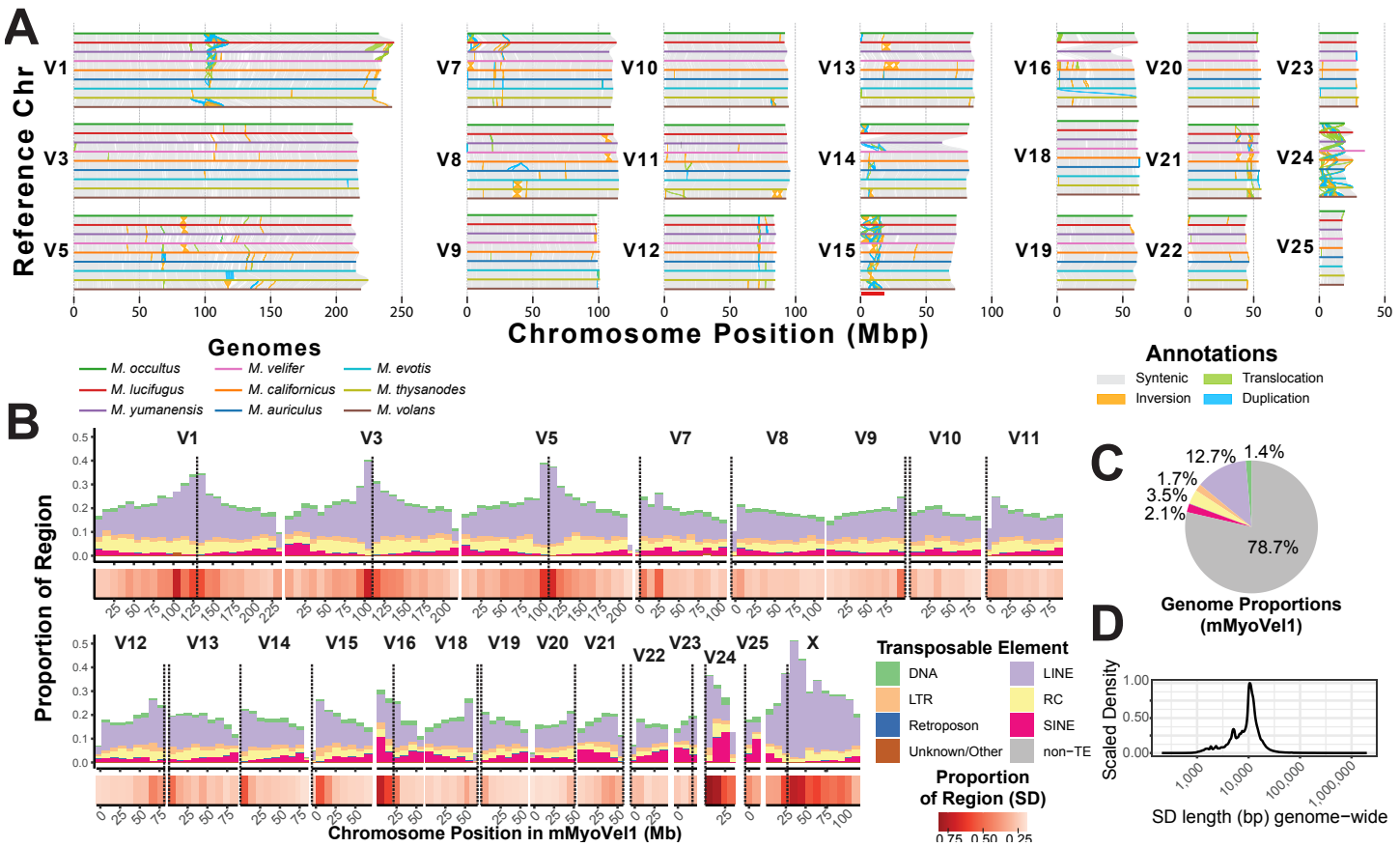
A
Reference Chr
V1
V3
V5
V7
V8
V9
V10
V11
V12
V13
V14
V15
V16
V18
V19
V20
V21
V22
V23
V24
V25
Chromosome Position (Mbp)
Genomes
M. occultus
M. lucifugus
M. yumanensis
M. velifer
M. californicus
M. auriculus
M. evotis
M. thysanodes
M. volans
Annotations
Syntenic
Inversion
Translocation
Duplication
B
Proportion of Region
X
Chromosome Position in mMyoVel1 (Mb)
Transposable Element
DNA
LTR
Retroposon
Unknown/Other
LINE
RC
SINE
non−TE
Proportion of Region (SD)
C
12.7%
1.4%
1.7%
3.5%
2.1%
78.7%
Genome Proportions (mMyoVel1)
D
Scaled Density
SD length (bp) genome−wide

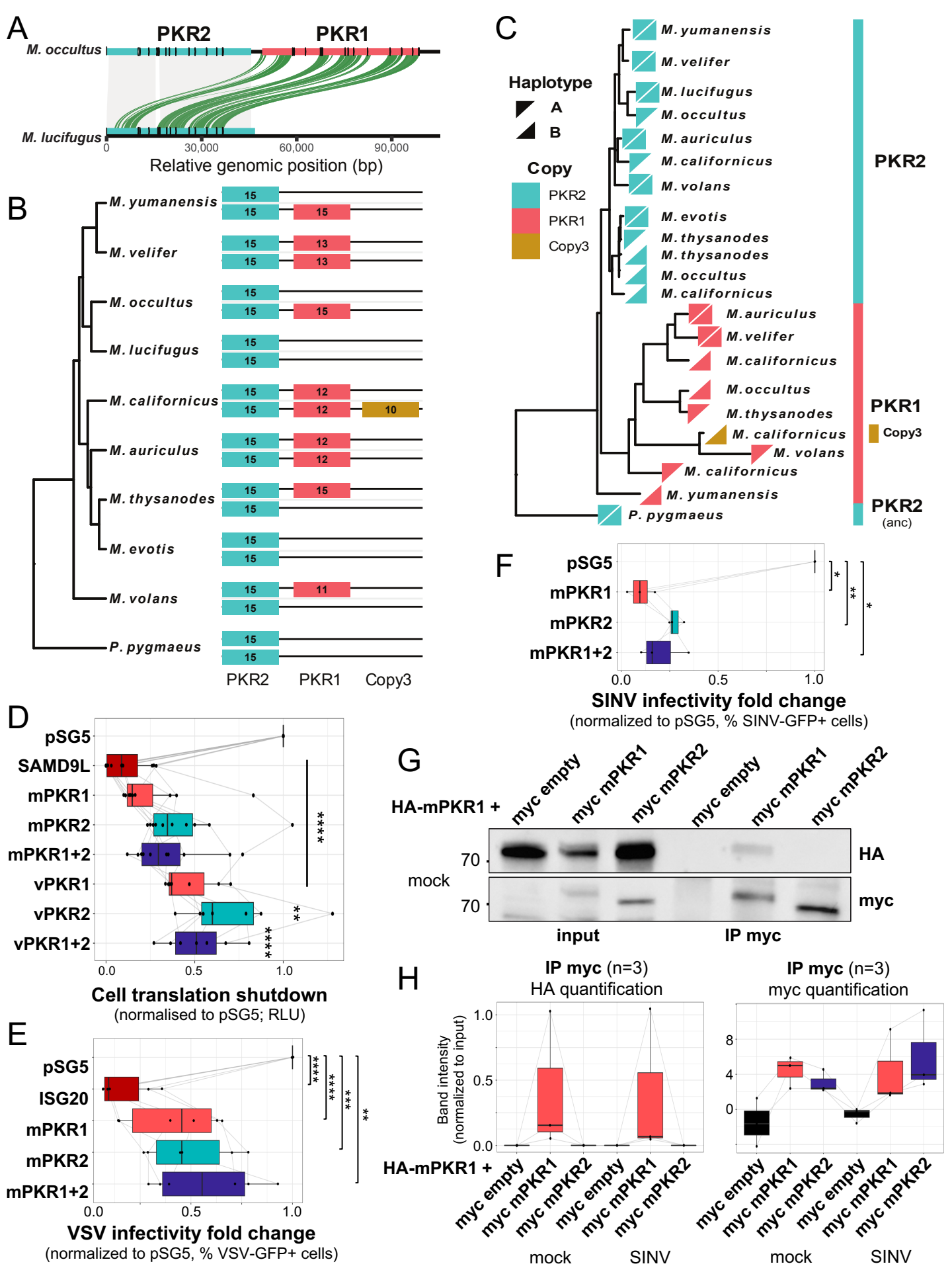
A
PKR2
PKR1
M. occultus
M. lucifugus
0
30,000
60,000
90,000
Relative genomic position (bp)
B
M. yumanensis
M. velifer
M. occultus
M. lucifugus
M. californicus
M. auriculus
M. thysanodes
M. evotis
M. volans
P. pygmaeus
PKR2
PKR1
Copy3
C
Haplotype
A
B
Copy
PKR2
PKR1
Copy3
M. yumanensis
M. velifer
M. lucifugus
M. occultus
M. auriculus
M. californicus
M. volans
M. evotis
M. thysanodes
M. thysanodes
M. occultus
M. californicus
M. auriculus
M. velifer
M. californicus
M. occultus
M. thysanodes
M. californicus
M. volans
M. californicus
M. yumanensis
P. pygmaeus
PKR2
PKR1
Copy3
PKR2
(anc)
D
pSG5
SAMD9L
mPKR1
mPKR2
mPKR1+2
vPKR1
vPKR2
vPKR1+2
Cell translation shutdown
(normalised to pSG5; RLU)
E
pSG5
ISG20
mPKR1
mPKR2
mPKR1+2
VSV infectivity fold change
(normalized to pSG5, % VSV-GFP+ cells)
F
pSG5
mPKR1
mPKR2
mPKR1+2
SINV infectivity fold change
(normalized to pSG5, % SINV-GFP+ cells)
G
HA-mPKR1 +
myc empty
myc mPKR1
myc mPKR2
myc empty
myc mPKR1
myc mPKR2
mock
70
70
HA
myc
input
IP myc
H
IP myc (n=3)
HA quantification
IP myc (n=3)
myc quantification
Band intensity
(normalized to input)
HA-mPKR1 +
myc empty
myc mPKR1
myc mPKR2
myc empty
myc mPKR1
myc mPKR2
mock
SINV

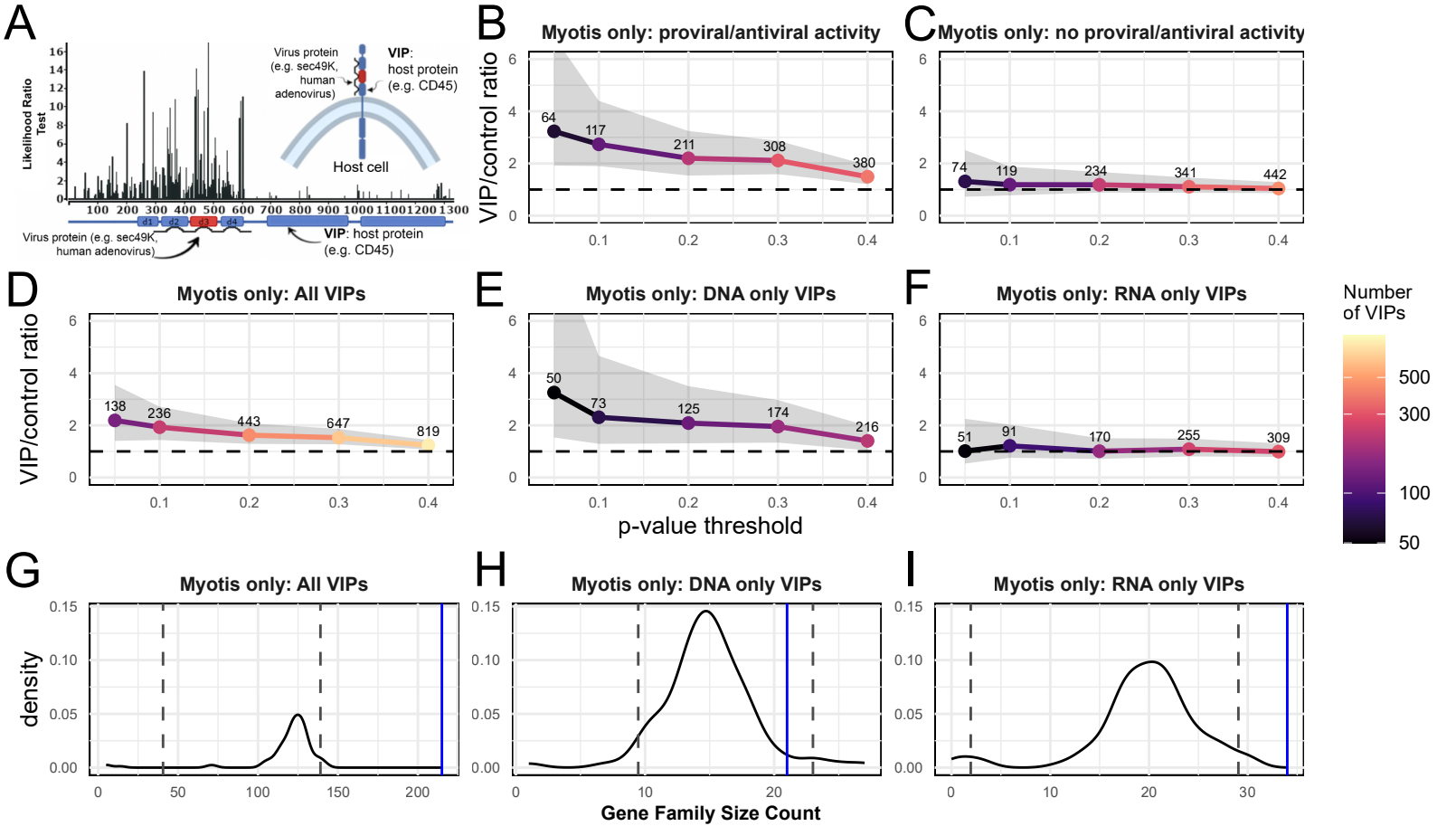
A
Likelihood Ratio Test
Virus protein (e.g. sec49K, human adenovirus)
VIP: host protein (e.g. CD45)
Host cell
d1
d2
d3
d4
Virus protein (e.g. sec49K, human adenovirus)
VIP: host protein (e.g. CD45)
B
Myotis only: proviral/antiviral activity
C
Myotis only: no proviral/antiviral activity
D
Myotis only: All VIPs
E
Myotis only: DNA only VIPs
F
Myotis only: RNA only VIPs
VIP/control ratio
p-value threshold
Number of VIPs
G
Myotis only: All VIPs
H
Myotis only: DNA only VIPs
I
Myotis only: RNA only VIPs
density
Gene Family Size Count

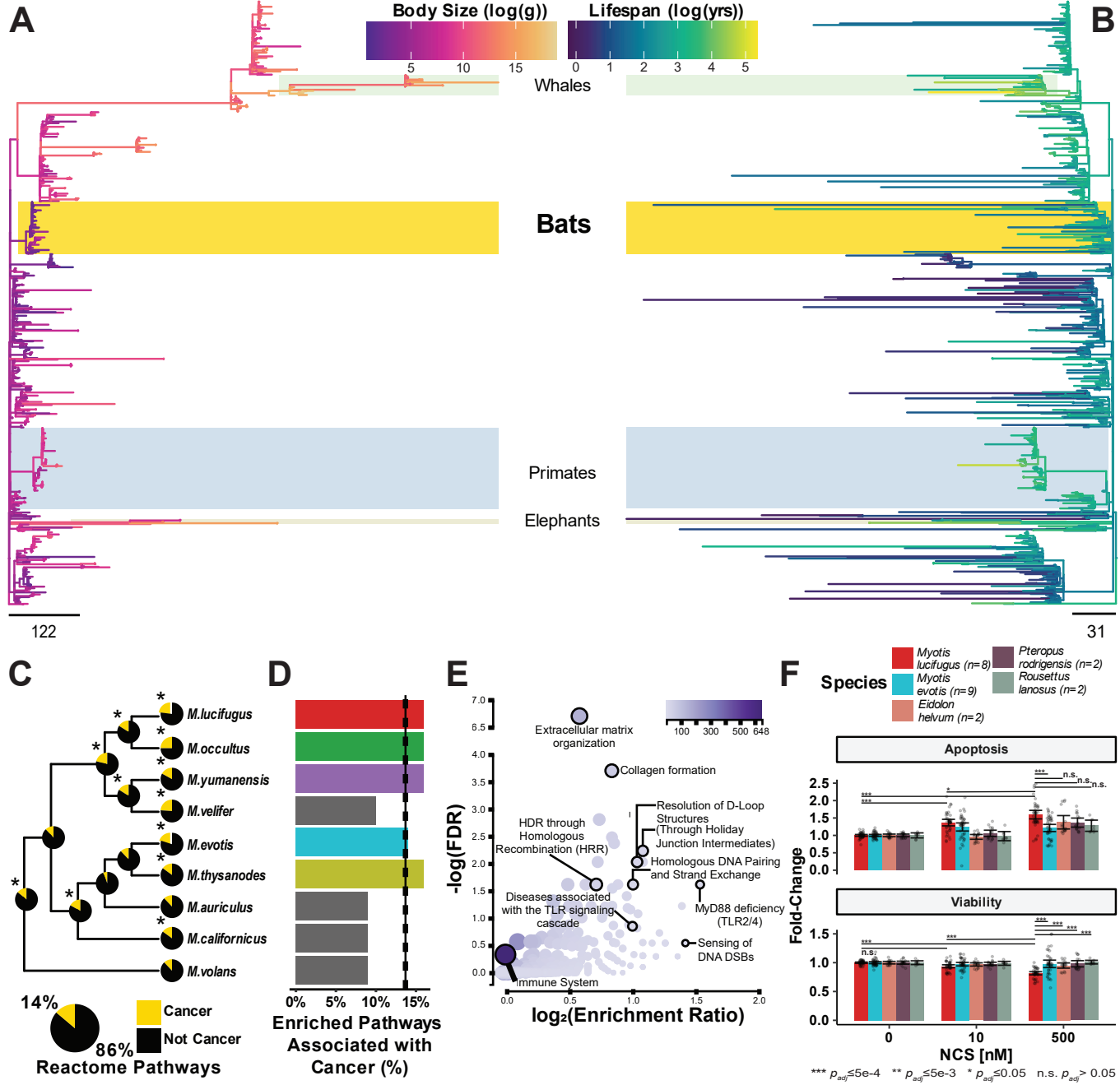
A
B
Body Size (log(g))
5
10
15
Lifespan (log(yrs))
0
1
2
3
4
5
Whales
Bats
Primates
Elephants
122
31
C
M.lucifugus
M.occultus
M.yumanensis
M.velifer
M.evotis
M.thysanodes
M.auriculus
M.californicus
M.volans
14%
86%
Cancer
Not Cancer
Reactome Pathways
D
0%
5%
10%
15%
Enriched Pathways Associated with Cancer (%)
E
Extracellular matrix organization
Collagen formation
Resolution of D-Loop Structures (Through Holiday Junction Intermediates)
Homologous DNA Pairing and Strand Exchange
HDR through Homologous Recombination (HRR)
Diseases associated with the TLR signaling cascade
MyD88 deficiency (TLR2/4)
Sensing of DNA DSBs
Immune System
100
300
500
648
-log(FDR)
log2(Enrichment Ratio)
F
Species
Myotis lucifugus (n=8)
Myotis evotis (n=9)
Eidolon helvum (n=2)
Pteropus rodrigensis (n=2)
Rousettus lanosus (n=2)
Apoptosis
Viability
Fold-Change
NCS [nM]
0
10
500
*** p_{adj}≤5e-4 ** p_{adj}≤5e-3 * p_{adj}≤0.05 n.s. p_{adj}> 0.05

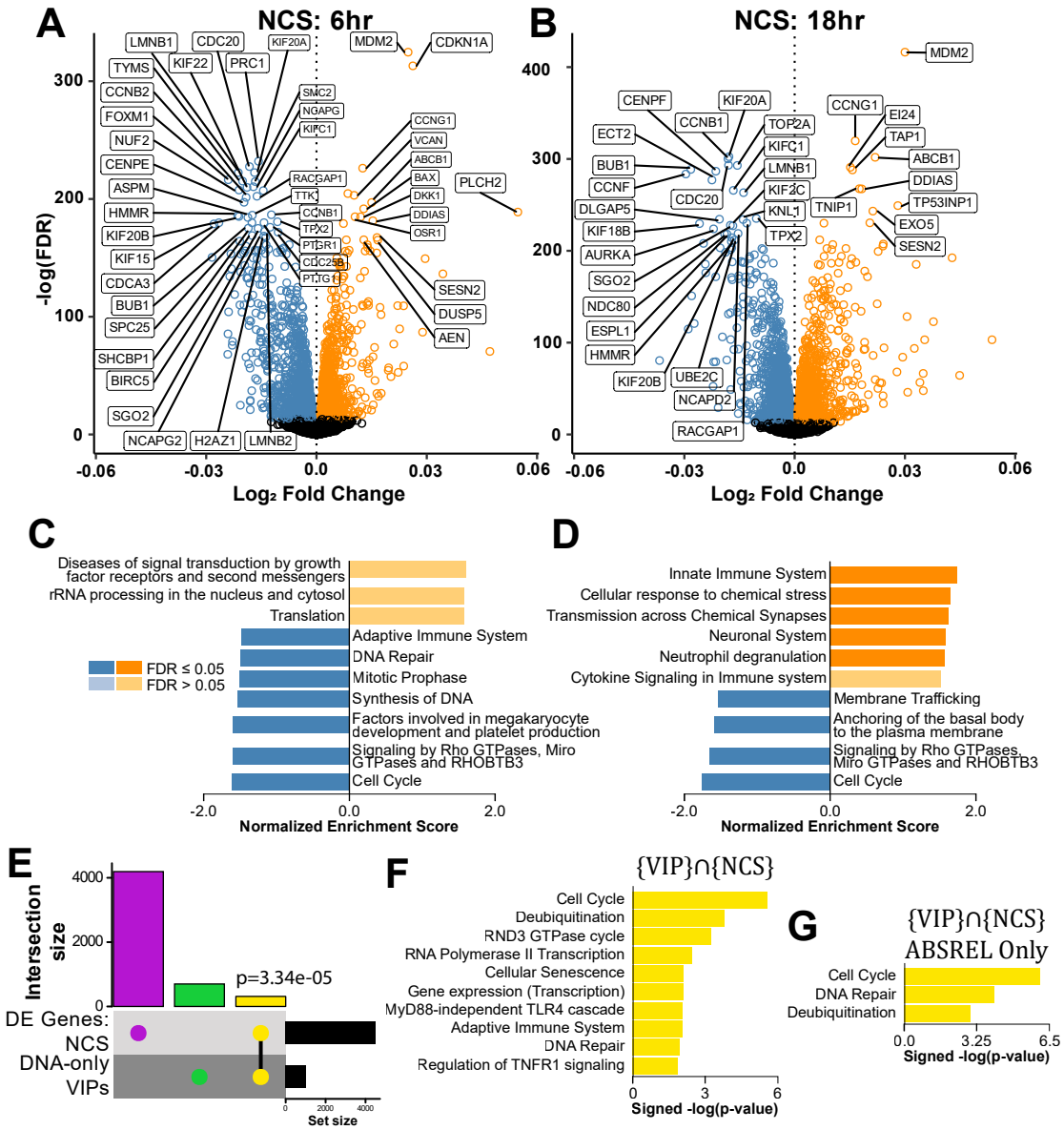
A
NCS: 6hr
-log(FDR)
Log₂ Fold Change
LMNB1
CDC20
KIF20A
MDM2
CDKN1A
TYMS
KIF22
PRC1
CCNB2
FOXM1
NUF2
CENPE
ASPM
HMMR
KIF20B
KIF15
CDCA3
BUB1
SPC25
SHCBP1
BIRC5
SGO2
NCAPG2
H2AZ1
LMNB2
SMC2
NCAPG
KIFC1
RACGAP1
TTK
CCNB1
TPX2
PTGR1
CDC25B
PTTG1
CCNG1
VCAN
ABCB1
BAX
DKK1
DDIAS
OSR1
PLCH2
SESN2
DUSP5
AEN
B
NCS: 18hr
Log₂ Fold Change
MDM2
CENPF
KIF20A
CCNB1
ECT2
BUB1
CCNF
CDC20
DLGAP5
KIF18B
AURKA
SGO2
NDC80
ESPL1
HMMR
KIF20B
UBE2C
NCAPD2
RACGAP1
TOP2A
KIFC1
LMNB1
KIF2C
KNL1
TPX2
CCNG1
EI24
TAP1
ABCB1
DDIAS
TP53INP1
TNIP1
EXO5
SESN2
C
Diseases of signal transduction by growth factor receptors and second messengers
rRNA processing in the nucleus and cytosol
Translation
Adaptive Immune System
DNA Repair
Mitotic Prophase
Synthesis of DNA
Factors involved in megakaryocyte development and platelet production
Signaling by Rho GTPases, Miro GTPases and RHOBTB3
Cell Cycle
FDR ≤ 0.05
FDR > 0.05
Normalized Enrichment Score
D
Innate Immune System
Cellular response to chemical stress
Transmission across Chemical Synapses
Neuronal System
Neutrophil degranulation
Cytokine Signaling in Immune system
Membrane Trafficking
Anchoring of the basal body to the plasma membrane
Signaling by Rho GTPases, Miro GTPases and RHOBTB3
Cell Cycle
Normalized Enrichment Score
E
Intersection size
p=3.34e-05
DE Genes:
NCS
DNA-only
VIPs
Set size
F
{VIP}∩{NCS}
Cell Cycle
Deubiquitination
RND3 GTPase cycle
RNA Polymerase II Transcription
Cellular Senescence
Gene expression (Transcription)
MyD88-independent TLR4 cascade
Adaptive Immune System
DNA Repair
Regulation of TNFR1 signaling
Signed -log(p-value)
G
{VIP}∩{NCS}
ABSREL Only
Cell Cycle
DNA Repair
Deubiquitination
Signed -log(p-value)